

**Rigidity percolation by next-nearest-neighbor bonds on generic and regular isostatic lattices**Leyou Zhang,<sup>1</sup> D. Zeb Rocklin,<sup>1,\*</sup> Bryan Gin-gé Chen,<sup>2</sup> and Xiaoming Mao<sup>1</sup><sup>1</sup>*Department of Physics, University of Michigan, Ann Arbor, Michigan 48109, USA*<sup>2</sup>*Instituut-Lorentz for Theoretical Physics, Leiden University, NL 2333 CA Leiden, The Netherlands*

(Received 20 December 2014; published 18 March 2015)

We study rigidity percolation transitions in two-dimensional central-force isostatic lattices, including the square and the kagome lattices, as next-nearest-neighbor bonds (“braces”) are randomly added to the system. In particular, we focus on the differences between regular lattices, which are perfectly periodic, and generic lattices with the same topology of bonds but whose sites are at random positions in space. We find that the regular square and kagome lattices exhibit a rigidity percolation transition when the number of braces is  $\sim L \ln L$ , where  $L$  is the linear size of the lattice. This transition exhibits features of both first-order and second-order transitions: The whole lattice becomes rigid at the transition, and a diverging length scale also exists. In contrast, we find that the rigidity percolation transition in the generic lattices occur when the number of braces is very close to the number obtained from Maxwell’s law for floppy modes, which is  $\sim L$ . The transition in generic lattices is a very sharp first-order-like transition, at which the addition of one brace connects all small rigid regions in the bulk of the lattice, leaving only floppy modes on the edge. We characterize these transitions using numerical simulations and develop analytic theories capturing each transition. Our results relate to other interesting problems, including jamming and bootstrap percolation.

DOI: [10.1103/PhysRevE.91.032124](https://doi.org/10.1103/PhysRevE.91.032124)

PACS number(s): 64.60.ah, 64.60.an, 62.20.F–

**I. INTRODUCTION**

Suppose we build a house or some other mechanical structure based on a square grid. Such a structure would be “shaky” in the following sense—each pair of adjacent rows or columns of walls can be sheared by only bending the material at the crossing points, and this has a much lower energy cost than compression or extension. If we insert a diagonal brace across a grid square, we will stabilize the structure by removing a shear mode from the system, *but how many braces do we need to stabilize the whole structure?*

This type of question belongs to a class of problems known as “rigidity percolation” [1–5]. In a typical rigidity percolation problem, one starts from a stable lattice, removes bonds randomly so each bond is present with probability  $p$ , and then examines the threshold probability  $p_r$  where the structure loses macroscopic mechanical stability and finally identifies corresponding scaling laws near this point. A variety of interesting phenomena have been identified in different versions of rigidity percolation, depending on the model system. In particular, each model is characterized by the location of the rigidity percolation critical point, the length scale that is associated with the emergence of the infinite rigid cluster, the way various elastic moduli grow from the rigidity percolation point, as well as how states of self-stress start to occur. Interestingly, instead of comprising a *single universality class*, rigidity percolation transitions are strongly affected by the lattice architecture and different classes of behaviors have been observed in different model systems. For example, rigidity percolation in diluted generic triangular lattices occurs at  $p_r^{\text{generic triangular}} = 0.6602 \pm 0.0003$  and displays a characteristic rigid cluster length scale that diverges as  $|p - p_r|^{-\nu}$  with exponent  $\nu = 1.21 \pm 0.06$  [5]. Here “generic” means the sites are not on a perfect periodic lattice, so rigidity only depends

on the connectivity, as we discuss in detail below. In contrast, in three dimensions (3D) [6] and on complete graphs [7–10], in which bonds are randomly added between any two vertices, the rigidity percolation transition is first order, as it is on Bethe lattices [11]. Moreover, the jamming of frictionless spheres, which can also be viewed as a version of self-organized rigidity percolation, exhibits mean-field scaling laws and a jump in coordination number and has been characterized as a “mixed first-and-second-order transition” [12–14]. So far, there are no universal theories that apply to all types of rigidity percolation.

A new category of rigidity percolation has been studied on periodic lattices that are at the verge of mechanical instability (called “isostatic lattices,” as discussed below), such as the square lattice discussed in the first paragraph. Random addition of next-nearest-neighbor (NNN) bonds (from now on known as *braces*) can remove “floppy modes” (i.e., deformations that do not change the length of any bond) in these lattices [15–20] and thus lead to a rigidity percolation transition. We will call this category of rigidity percolation problems “bracing percolation.” Previously, the rigidity percolation transition in a braced generic square lattice was found to be first-order in Ref. [20]. In the treatment of that paper, the system was pinned along two *diagonal* edges and free along the other two diagonals. As we will see, the boundary plays a crucial role in the rigidity transition, and our system’s open boundaries lead to qualitatively new behavior while confirming the essential order of the transition.

To understand the unique features of bracing percolation, it is useful to review how one determines whether a structure has mechanical stability. Consider normal modes of a  $d$ -dimensional system. The zero-energy modes of this  $d$ -dimensional system can be divided into  $d(d + 1)/2$  rigid-body translations and rotations of the whole system and  $F$  floppy modes which involve relative displacements between different parts of the system. J. C. Maxwell noted in 1864 [15] that for

\*Corresponding author: drocklin@umich.edu

a system of  $N$  particles and  $N_c^{(i)}$  independent constraints,

$$F = dN - N_c^{(i)} - \frac{d(d+1)}{2}. \quad (1.1)$$

The system then becomes rigid (mechanically stable) when  $F = 0$ , at the *isostatic point*. Under this *Maxwell behavior*, each bond placed in the system eliminates a single floppy mode until the system becomes rigid when the number of constraints is

$$dN - \frac{d(d+1)}{2}. \quad (1.2)$$

However, in general and as discussed below, some bonds may be redundant and generate self-stresses rather than eliminating floppy modes. This leads to the modified Maxwell relationship [21],

$$F = dN - N_c - \frac{d(d+1)}{2} + S, \quad (1.3)$$

where the number of floppy modes depends not only on the number of constraints  $N_c$  but also on  $S$ , the number of self-stresses in the system. These self-stresses not only determine rigidity but are determined by it—a self-stress occurs when a bond connects two sites in a rigid region of the structure. This modified Maxwell’s rule has been shown to be an index theorem for topological surface modes in systems near isostaticity [22].

Large central-force lattices with coordination number  $z = 2d$  are called “isostatic lattices” because in the bulk each site has equal numbers of degrees of freedom and constraints (assuming central-force nearest bonds only) [19,23]. A finite piece of an isostatic lattice has  $F \propto L^{d-1}$ , where  $L$  is the linear size of the lattice and  $N \sim L^d$ , because sites on the boundary have fewer than  $2d$  bonds. To make such a finite lattice stable, one could add exactly  $F$  braces by making sure that they are all independent, and thus all floppy modes are eliminated. We can thus define the “Maxwell number”  $N_M$  of a finite isostatic lattice, the minimum number of braces needed to rigidify the lattice if all braces were added independently.

If the braces are instead added randomly, how many does one typically need for rigidity? Studies of bracing percolation on isostatic lattices address this question. It is worth pointing out that unlike other rigidity percolation problems, the rigidity of isostatic lattices is strongly affected by boundary conditions because isostatic lattices have a subextensive number of floppy modes due only to their boundary. The above discussion refers to lattices with open boundary conditions. Changing to periodic boundary condition may or may not lift the floppy modes, depending on the architecture of the lattice [24].

In particular, in Ref. [17] it was shown that the bracing percolation problem on the regular 2D square lattice, which is an example of an isostatic lattice, can be mapped into a random graph problem (see also Ref. [25]). Thus exact solutions are possible; it was found that if each brace is present with a uniform probability  $p$ , rigidity percolation in a (regular) periodic square lattice of size  $L \times L$  occurs at

$$p_r^{\text{regular square}} = \frac{\ln L}{L} + \mathcal{O}(1/L), \quad (1.4)$$

where “regular” refers to perfectly periodic lattices (see discussions below). At this transition, the probability of a site to be part of the infinite rigid cluster jumps from 0 to 1. On the other hand, the form of  $p_r$  suggests a length scale

$$\xi^{\text{regular square}} \sim p^{-1}, \quad (1.5)$$

corresponding to a characteristic system size that exhibits with high probability mechanical stability at a given  $p$ .

Interestingly, this scaling relation for the length scale, together with a characteristic frequency  $\omega^* \sim p$  [16], agrees with corresponding scaling relations observed near jamming [26,27], namely

$$\omega^* \sim \Delta z, \quad l^* \sim \Delta z^{-1}, \quad (1.6)$$

where  $\Delta z = \langle z \rangle - 2d$  is the coordination above isostaticity and thus the same as  $p$ . These scaling relations differ from those observed in randomly diluted triangular lattices [5] but agree with those of randomly braced isostatic lattices.

The above results on square lattices are derived for perfectly periodic square lattices, in which lattice sites sit on a periodic square grid in space and bonds in each row or column are collinear [24,28,29]. However, real physical lattices invariably have sites displaced slightly from regular lattice positions, and these displacements profoundly alter the rigidity of the system. As pointed out in Ref. [5], perfect periodic lattices may exhibit self-stress because some bonds may be redundant because they are parallel to each other, and thus to study the fundamental physics of rigidity percolation one should eliminate such redundancy coming from the symmetry of the lattices by randomizing the positions of the lattice sites. Floppy modes in these randomized lattices depend only on the lattice’s topology rather than the positions of the sites [30] and these lattices lack the straight lines which allow stress to be transmitted over long distances without decaying and thus may exhibit generic properties of rigidity transitions that depend only on the network’s connectivity. Here we follow the terminology of Ref. [5] and call the perfect periodic lattices “regular” and the randomized versions “generic.” The rigidity of the generic lattices can be determined by a fast algorithm called the “pebble game” [5,31,32] which is based on Laman’s theorem for the rigidity of 2D graphs [33]. We also use this algorithm to determine the rigidity of generic isostatic lattices.

Studies on the regular square lattice reveal interesting physics that is intimately related to jamming, but jamming involves random packings not living on lattices. It is thus of interest to examine what changes if one considers generic rather than regular square lattices.

In this paper, we compare rigidity percolation transitions in braced regular [Figs. 1(a) and 1(b)] and generic [Figs. 1(c) and 1(d)] isostatic lattices. We investigate how generic and regular square and kagome lattices, which have  $N_M \sim \mathcal{O}(L)$  floppy modes when no braces are present, gain rigidity as braces are randomly added to these lattices.

In particular, instead of having each brace present with a probability  $p$ , we use the total number of braces  $N_b$  as our control parameter. In other words, we consider the process of randomly adding braces into the lattice one by one. This is because we find that the rigidity percolation transition in the generic isostatic lattices is an extremely sharp first-order transition, and using fixed  $p$  broadens the transition window

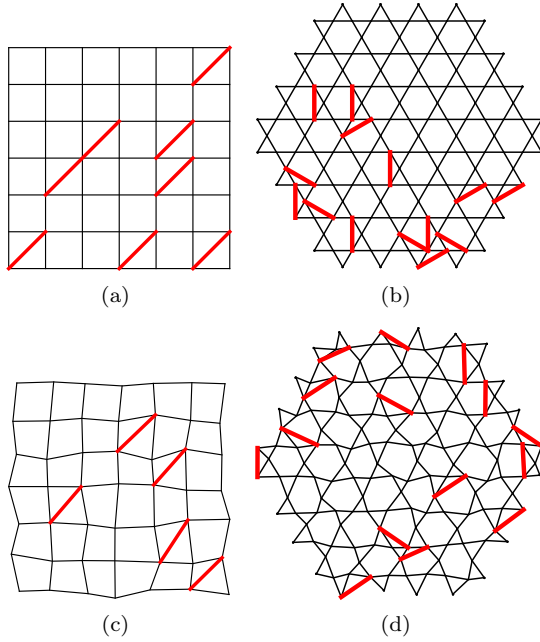


FIG. 1. (Color online) Illustration of regular square (a), regular kagome (b), generic square (c), and generic kagome lattices (d) with nearest-neighbor (NN) bonds (black, thin) and random NNN braces (red, thick). The square lattices depicted have  $L = 7$  and the kagome lattices have  $L = 4$ .

and obscures the sharpness of the transition, as we discuss below.

Our main results are as follows:

(i) Both regular square and kagome lattices show a rigidity percolation transition occurring when the number of randomly added braces  $N_b = N_{b,r} \propto L \ln L$ , where  $L$  is the linear size. This transition shows features of both first-order and second-order transitions, sharing similarities to many other interesting systems [13,14,34–38]. In addition, both of these two lattices exhibit another transition at a lower density of braces, at  $N_{b,g} \propto L$ , at which the number of floppy modes shows certain singularities. Our numerical results and analytical theory for these phenomena show good agreement.

(ii) Both the generic square and kagome lattices show a very sharp, first-order-like rigidity transition, in contrast to that of the regular lattices. In particular, as braces are randomly added to the generic lattice, floppy modes are eliminated, following Maxwell’s rule [Eq. (1.1)] perfectly without any states of self-stress ( $S = 0$ ), until the number of braces,  $N_b$ , becomes close to the total number of floppy modes,  $N_M - N_b \lesssim \mathcal{O}(1)$ , when the bulk of the lattice suddenly rigidifies (which we name “bulk rigidity”) as a single brace is added, leaving only  $\lesssim \mathcal{O}(1)$  floppy modes on the *boundary of the lattice*. After this point, states of self-stress start to develop, and, within  $\mathcal{O}(1)$  more braces, the whole lattice becomes rigid with finite probability. This greatly differs from regular lattices in which states of self-stress develop before an infinite rigid cluster appears, and it requires  $\mathcal{O}(L \ln L)$  bonds to rigidify the system.

In Sec. II we define the models we study and present our results from numerical simulations, using the “pebble game” algorithm and direct calculations by evaluating ranks

of rigidity matrices. In Sec. III we present theoretical results on the number of floppy modes and the probability of rigidity as functions of the number of added braces in regular isostatic lattices. In Sec. IV we present theoretical results for generic isostatic lattices, including edge modes and statistics of rigidity. In Sec. V we summarize our conclusions and discuss the relation of our work to other studies.

## II. SIMULATION RESULTS

We begin by defining the family of random spring networks that we study.

For a square lattice with  $L$  sites per side, initially there are a total of  $N = L^2$  particles,  $2L^2 - 2L$  bonds, and  $2L - 3$  floppy modes, so  $N_M = 2L - 3$  [see Fig. 1(a)]. We add random braces, with only one choice of brace permitted in each plaquette (bottom left to upper right in the figures we show), as a second such brace (upper left to bottom right) is always redundant if the first one is present. There are then  $(L - 1)^2$  places braces may be placed.

For the kagome lattice, we study systems shaped like large hexagons with  $L$  hexagons per side [see Fig. 1(b)]. There are  $N = 9L^2 + 3L$  particles and initially  $18L^2$  bonds and  $F = 6L - 3$  floppy modes on the kagome lattices, and thus  $N_M = 6L - 3$  as well. We then add random braces. For kagome lattices, again we allow only half of the brace positions as the other half are redundant. Thus for each hexagon, three independent bracing positions are allowed. There are then  $9L^2 - 3L$  places braces may be placed.

For these lattices, we generate realizations of disorder by randomly adding  $N_b$  braces and mainly evaluate two important quantities:  $\mathcal{P}_{\text{rigid}}$ , denoting the probability the lattice is rigid (i.e., has no floppy modes), and  $\langle F \rangle$ , denoting the average number of floppy modes, to characterize the rigidity of the lattice. As we explain below for the two cases of regular and generic lattices, having no floppy modes is equivalent to having a rigid cluster that percolate through the whole system (rigidity percolation). We use different computational methods to determine the rigidity of the regular and the generic lattices, as we discuss in detail below.

### A. Determining rigidity of regular lattices

The infinitesimal rigidity properties of a spring network can be determined from the “rigidity matrix” (or compatibility matrix) [21]. This is an  $N_c \times dN$  matrix  $\mathbf{R}$  which computes the vector of bond extensions  $e$  from the vector of particle displacements  $u$ , i.e.,  $e = \mathbf{R} \cdot u$ . The rank of  $\mathbf{R}$  gives the number of independent constraints on the  $dN$  degrees of freedom, and so the dimension of the space of infinitesimal displacements of the particles which do not stretch any bonds to first order is the dimension of the null space of  $\mathbf{R}$ , so in two dimensions

$$F = 2N - 3 - \text{rank}(\mathbf{R}). \quad (2.1)$$

For the regular lattices, there exist simplified rigidity matrices, which we call “braced rigidity matrices.” They contain  $N_b$  rows and approximately  $N_M$  columns. This simplification from  $\mathcal{O}(L^2)$  columns to  $\mathcal{O}(L)$  columns is because the floppy modes for the unbraced regular square lattice and the unbraced regular kagome lattice can be written in a convenient “line-localized”

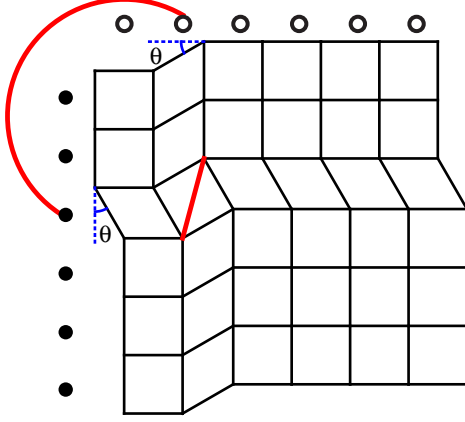


FIG. 2. (Color online) One example of the mapping of braced regular square lattices to bipartite graphs. In this mapping floppy modes in the “line-localized” basis, taking the form of shearing rows (columns), are mapped to black (white) nodes, and braces are mapped to edges (solid red curve) connecting the two types of nodes. The deformation of this regular square lattice illustrates how the brace locks the two floppy modes together.

basis. The prototype is the regular square lattice with braces, whose braced rigidity matrix arises from the mapping of its rigidity properties to bipartite graphs, as shown in Fig. 2 (described in Refs. [17,25], see also Sec. III). Via this mapping, the rigidity of a set of braces can be determined from the incidence matrix of an associated bipartite graph [25], which is the braced rigidity matrix in this case. This bipartite graph has  $2L - 2 = N_M + 1$  vertices, one for every adjacent pair of rows or columns, and one edge for every brace. For the regular kagome lattice the braced rigidity matrices are  $N_b \times (6L)$  matrices whose construction is outlined in Appendix B.

Thus, for regular lattices, we first calculate  $\langle F \rangle$  (averaged over random configurations of braces) by calculating the ranks of the braced rigidity matrices after adding  $N_b$  independent and randomly distributed braces. We then find  $\mathcal{P}_{\text{rigid}}$  by calculating the probability of having  $F = 0$  among all the realizations. Because all floppy modes are extended row or column modes, rigidity percolation coincides with  $F = 0$ . For the regular square lattices, we studied  $\langle F \rangle$  in systems with linear system sizes  $L = 100, 200, 300$  and averaged over  $10^3$  configurations. To study  $\mathcal{P}_{\text{rigid}}$  we looked at regular square lattices with  $F = 0$  and  $L = 320, 640, 1280$ . For the regular kagome lattices, we studied systems with sizes ranging from  $L = 100$  to  $L = 800$ , averaging over  $10^4$  configurations.

In order to study the spatial pattern of rigidity in regular lattices, we calculate the dynamical matrix [39] (the null space of which correspond to the floppy modes) of the regular square and kagome lattices to find the rigid plaquettes in the regular square lattices and the rigid hexagons in the regular kagome lattices. Self-stressed bonds in the regular square and kagome lattices are identified by checking whether removing such a bond creates a floppy mode.

We plot our data for  $\mathcal{P}_{\text{rigid}}$  for the regular square and kagome lattices in Fig. 3, data for  $\langle F \rangle$  in Fig. 4. Snapshots of regular square and kagome lattices with various numbers of added braces are shown in Fig. 8 with our discussion on the rigidity transition in generic lattices.

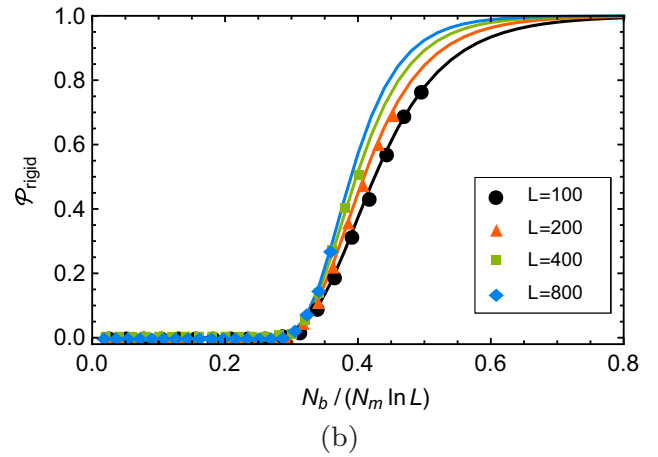
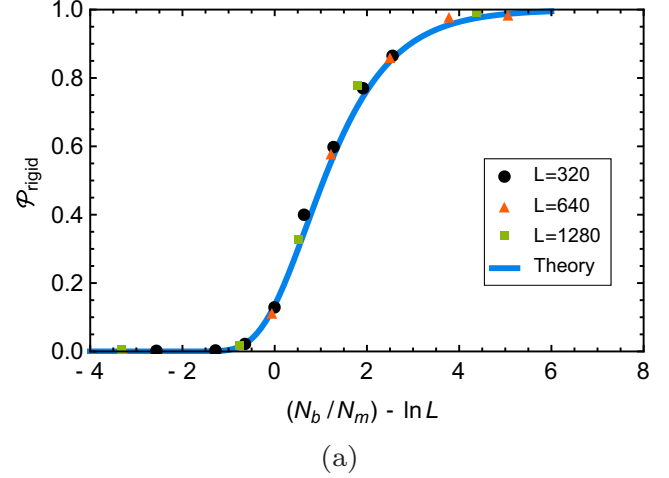


FIG. 3. (Color online) Probability  $\mathcal{P}_{\text{rigid}}$  for rigidity percolation in braced regular square (a) and kagome (b) lattices as a function of scaled number of braces. The curve in (a) shows the analytical asymptotic result in Eq. (3.3). The curves in (b) show the analytical result of Eq. (3.5). Error bars are smaller than the symbols.

The collapse of the plots of  $\mathcal{P}_{\text{rigid}}$  at different lattice sizes onto a single line in Fig. 3 shows that the rigidity transitions in regular square and kagome lattices occur at

$$N_{b,r}^{\text{regular}} \propto L \ln L, \quad (2.2)$$

in agreement with result of  $p_r^{\text{regular square}}$  in Eq. (1.4) from Ref. [17], because the probability of having each brace and the (average) total number of braces are related by  $\langle N_b \rangle = p(L-1)^2$ .

In addition, our data for  $\langle F \rangle$  (Fig. 4) indicate that, before the whole system becomes rigid, there is another transition at

$$N_{b,g}^{\text{regular}} \propto N_M \propto L. \quad (2.3)$$

This is identified from a singularity in  $\langle F \rangle$  and is associated to the emergence of a giant cluster of locked floppy modes (which is not sufficient to rigidify the whole lattice), as detailed in Sec. III.

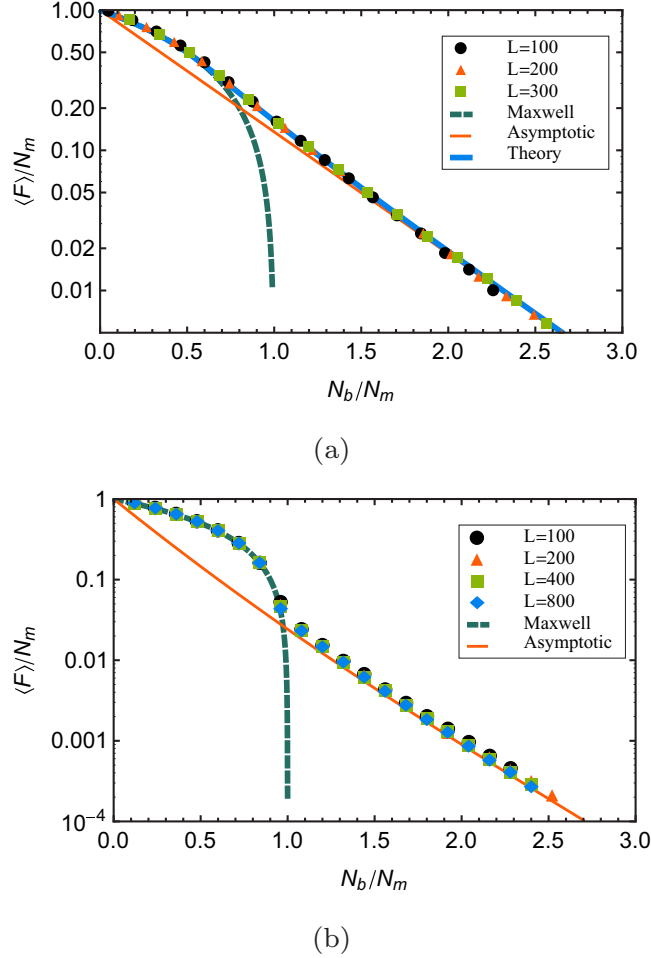


FIG. 4. (Color online) Average number of floppy modes normalized by the Maxwell number  $\langle F \rangle / N_M$  of braced regular square (a) and kagome (b) lattices as a function of  $N_b / N_M$ . The asymptotic line in (a) is from Eq. (3.9) and the theory line in (a) is from Eq. (3.10). The asymptotic line in (b) is from Eq. (3.11). Error bars are smaller than symbols.

### B. Determining rigidity of generic lattices

For generic lattices, instead of generating rigidity matrices, we use the “pebble game” algorithm, developed in Refs. [5,31,32] and based on Laman’s theorem [33], to count the number of floppy modes and identify rigid regions and regions with states of self-stress (overconstrained regions). We study generic square and kagome lattices with  $N$  ranging from  $10^4$  to  $1.6 \times 10^5$ . For each  $N$ , we generate  $10^4$  realizations of random distribution of braces.

For each  $N_b$ , we calculate the average number of floppy modes  $\langle F \rangle$  and the probability for the whole lattice to be rigid  $\mathcal{P}_{\text{rigid}}$ , i.e., to have  $F = 0$ . As with the regular lattices, the last floppy modes of the generic lattices spread across the system, and so rigidity percolation is not achieved until  $F = 0$ .

From the simulation results, we find that the threshold for rigidity percolation is at

$$N_{b,r}^{\text{generic}} = N_M \propto L, \quad (2.4)$$

which occurs much earlier than the rigidity threshold in regular lattices as shown in Eq. (2.2) [40]. As  $N_b$  increases below

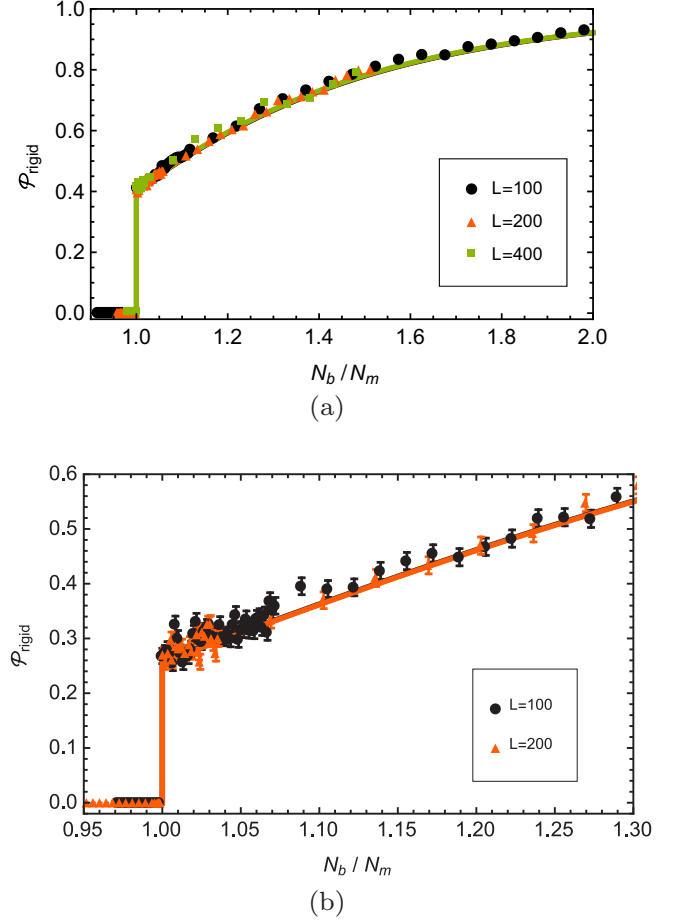


FIG. 5. (Color online) Probability of rigidity percolation  $\mathcal{P}_{\text{rigid}}$  on (a) generic square lattices and (b) generic kagome lattices as a function of  $N_b / N_M$ .  $\mathcal{P}_{\text{rigid}}$  remains zero until jumping to a finite value at the Maxwell point, indicating a first-order-like transition. The solid lines show the theoretical result of Eq. (4.12). Error bars smaller than the symbols are not shown.

$N_M$ ,  $\mathcal{P}_{\text{rigid}} = 0$  and  $\langle F \rangle$  decreases linearly with slope  $-1$ , following the Maxwell behavior of Eq. (1.1). At  $N_b = N_M$ ,  $\mathcal{P}_{\text{rigid}}$  discontinuously jumps to a finite value, and  $\langle F \rangle$  also exhibits a singularity, due to the sudden appearance of a rigid bulk. Beyond  $N_M$ ,  $\mathcal{P}_{\text{rigid}}$  continues to increase, while  $\langle F \rangle$  decreases exponentially to zero. As shown in Figs. 5 and 6, our data for  $\langle F \rangle$  and  $\mathcal{P}_{\text{rigid}}$  plotted as functions of  $N_b / N_M$  collapse at and above the Maxwell point. This behavior is explained by our analytical theory in Sec. IV.

Figure 7 depicts a sequence of images showing floppy, rigid, and overconstrained regions in generic lattices as  $N_b$  increases, illustrating the sudden emergence of a rigid bulk through the addition of only a single brace [from Fig. 7(a) to Fig. 7(b) in the generic square lattice and from Fig. 7(e) to Fig. 7(f) in the generic kagome lattice]. To provide a comparison, we also include snapshots of rigidity percolation in regular lattices in Fig. 8 (see videos [41]). Note the appearance of self-stresses in the regular square lattice well before  $N_M$  braces have been added. In the other lattices, a giant rigid component appears near  $N_b = N_M$ , leaving at most several floppy modes at the edge, which then are removed with the placement of further

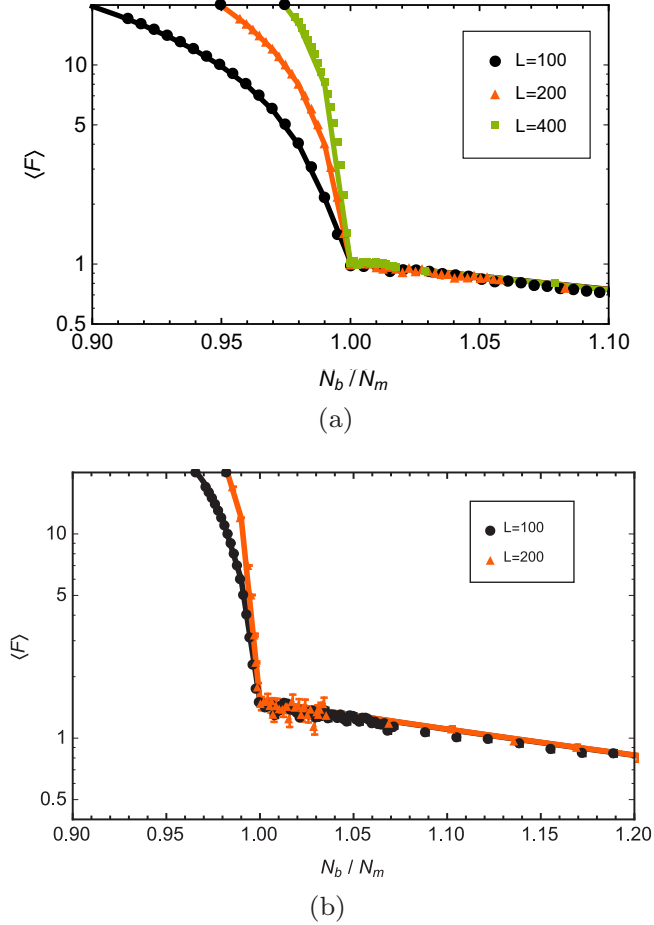


FIG. 6. (Color online) Average number of floppy modes  $\langle F \rangle$  of (a) generic square and (b) generic kagome lattices as a function of  $N_b/N_M$  on a semilog plot. The solid lines show the theoretical result of Eq. (4.11). There is a discontinuous change in slope at the Maxwell point  $N_M$ . Below  $N_M$ ,  $\langle F \rangle$  is proportional to  $L$ , but above  $N_M$ ,  $\langle F \rangle$  no longer scales with  $L$ . Error bars smaller than the symbols are not shown.

braces. For the small lattices used in the movies, the difference in the rigidity transitions between the regular kagome lattices [Eq. (3.6)] and generic kagome lattices [Eq. (4.12)] is not generally visible.

### III. THEORY OF RIGIDITY PERCOLATION IN REGULAR ISOSTATIC LATTICES

#### A. Basics of the theory

In this section we go into detail on rigidity transitions in bracing percolation on regular lattices. These lattices are nongeneric in the sense that there are graphs on the same set of vertices where the rigidity matrix does not have the maximum possible rank. If a randomly braced regular lattice is rigid, then the corresponding generic lattice with the same connectivity is also rigid, but the converse does not always hold.

One special property of the braced regular *square lattice* is that its rigidity properties map onto the connectivity properties of an associated bipartite graph [17,25]. The mapping begins

with the observation that an explicit independent (though not orthogonal) basis for the vector space of zero modes of a regular square grid of side length  $L$  consists of the two global translations as well as  $2L - 2$  shears of columns and rows [i.e., modes consisting of translations  $(0,1)$  of all vertices with  $x \geq j$  (shear of column  $j$ ) or translations  $(1,0)$  of all vertices with  $y \geq k$  (shear of row  $k$ )].

Setting aside the translational modes for now, we assign one vertex of an associated graph to each of the shear modes (Fig. 2). A brace constraint in the  $(j,k)$ <sup>th</sup> plaquette couples the shear of column  $j$  and the shear of row  $k$ . In the associated graph, we add the edge joining the two corresponding vertices. With this construction, the (nontranslational) floppy modes of the braced grid are in correspondence with the connected components of the associated graph.

Note that the constructed graph is bipartite, as each potential brace couples one row shear to one column shear. In fact, the random bracing process on a square grid maps to an Erdős-Rényi process on the complete bipartite graph  $K_{L-1,L-1}$  [17].

For regular kagome lattices, there is no such mapping. However, as explained in Appendix A, and exploited in our simulations described in Sec. II, we can still find a line-localized basis of independent zero modes where the displacements for each of these modes are localized onto particles on separate straight lines in the kagome lattice. This basis has the advantage that each brace couples only four modes together, which allows us to analyze the rigidity of the regular kagome via the interaction of independent braces on the line modes.

As mentioned in Sec. II A, the two observables  $\mathcal{P}_{\text{rigid}}$  and  $\langle F \rangle$  undergo two *distinct* transitions in braced regular lattices. Following Ref. [17], the rigidity percolation transition can be defined as the point where  $\mathcal{P}_{\text{rigid}}$  exceeds  $1/2$ . As we discuss below, this occurs in the regular kagome lattice when the number of added braces  $N_{b,r} \sim L \ln L$ , which is the same as the result found for regular square lattices [17] and explains our observation from simulation in Sec. II A.

The other transition occurs at a lower  $N_b$  where the number of floppy modes has a singularity in the large  $L$  limit when the number of added braces  $N_{b,r} \sim L$ . The nature of this singularity differs in the regular square and regular kagome lattices, so we describe them in turn here.

Previous work has suggested that the number of floppy modes is the analog of a “free energy” in rigidity percolation systems [11]. Indeed, in the aforementioned mapping between the regular square lattice with braces and bipartite graphs, the number of floppy modes in this rigidity percolation problem maps precisely to the number of connected components in a connectivity percolation problem. Thus, in the regular square lattice there is a singularity in  $\langle F \rangle$  corresponding to the formation of a giant component in the associated bipartite graph, and it occurs at

$$N_{b,g}^{\text{regular square}} = N_M/2, \quad (3.1)$$

well *before* the Maxwell point. We will show that this occurs via a second-order mean-field transition, and in fact the singularity is actually a discontinuity in the *third* derivative of  $\langle F \rangle$ , which is not visible in Fig. 4(a).

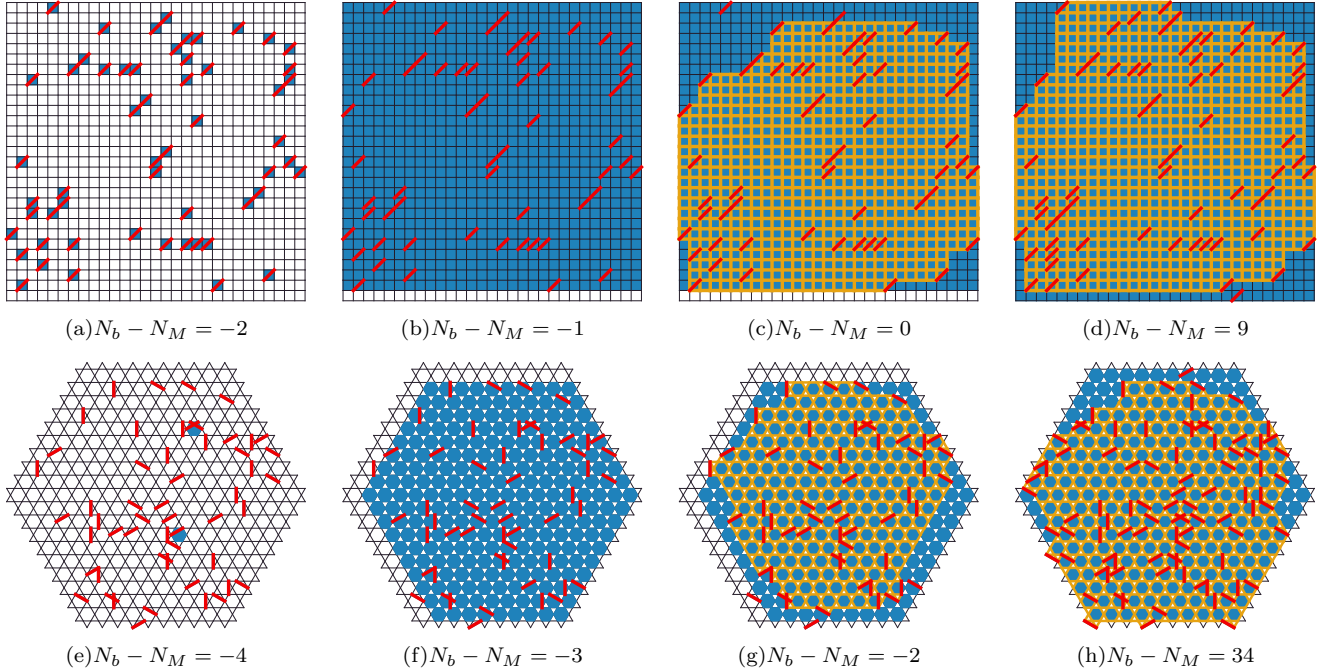


FIG. 7. (Color online) Snapshots of generic square [(a)–(d)] and kagome lattices [(e)–(h)] with the generic site displacements unpictured for visual clarity. Randomly placed braces are shown as red lines, rigid regions as blue areas, and stressed bonds as yellow lines. In (a) and (e), as braces are added they induce rigidity only locally. In (b) and (f) a single bond near the Maxwell point has induced rigidity in the bulk of the system, with at most  $\mathcal{O}(L)$  floppy plaquettes on the edge. As additional braces are added self-stresses are generated in the bulk, as shown in (c) and (g). It is only well above the Maxwell point, as shown in (d) and (h), that the floppy modes on the edge are completely eliminated. A video of rigidity percolation in the square lattice is included as Supplemental Material [41].

In the regular kagome lattice, the situation rather differs. There is a visible kink in  $\langle F \rangle / L$  at the Maxwell point [Fig. 4(b)],

$$N_{b,g}^{\text{regular kagome}} = N_M. \quad (3.2)$$

This indicates a first-order transition there, which is associated to the formation of a single giant rigid cluster.

The reason that there are two distinct transitions in the regular lattices is because sets of braces can form redundancies fairly easily. The coupling of a large number of floppy modes together is not sufficient to *completely* rigidify the system. In the regular square lattice, this coupling does not even create a single large rigid component, though it does for the regular kagome lattice. Despite the fact that most of the floppy modes become coupled together, many floppy modes remain “isolated”—that is, decoupled from all other modes—and added braces tend to create redundancies rather than remove degrees of freedom. In the bipartite graph representation of the regular square lattice, these floppy modes correspond indeed to isolated vertices, and adding enough braces to the system to couple them all to the giant floppy mode yields a coupon-collector problem [42]. The rigidity transition in the regular kagome lattice proceeds through a similar, but more complicated, process. Thus, in both cases, there is a separate transition to rigidity of the system which occurs much later: when  $p \sim \ln L / L$ .

Note that in both transitions there are system sizes which diverge with  $1/p$  (to lowest order) as the probability goes to

zero, below which the system is very floppy and above which the system is rigid.

### B. Probability of rigidity in regular lattices

We first describe the situation for the regular square lattice, giving a heuristic derivation of the results of Ref. [17]. Next, using those ideas, we conjecture a generalization for the regular kagome lattice which conforms closely to our simulation results with no free parameters. The probability of rigidity in a regular square lattice is simply the probability that there is a single connected component of the Erdős-Rényi model. This is asymptotically equal for large  $L$  to the probability of having at least one brace in every row and column of plaquettes [43]. Though this is a necessary rather than sufficient condition for rigidity [17], the probability of having a nonrigid configuration satisfying this condition goes to zero as the system size gets large.

Assuming this, and neglecting the slight dependence between the events of having a brace in a row and having a brace in a column, the probability that the configuration is rigid is the product over all rows and all columns of the probability that there is at least one brace in that row or column:

$$\begin{aligned} \mathcal{P}_{\text{rigid}}(p) &= \prod_{i \text{ rows, columns}} [1 - (1 - p)^{L-1}] \\ &= [1 - (1 - p)^{L-1}]^{2L-2} \approx e^{-2Le^{-pL}}. \end{aligned} \quad (3.3)$$

The underlying probabilistic process resembles that of the coupon-collector problem [42], where, supposing there are  $n$

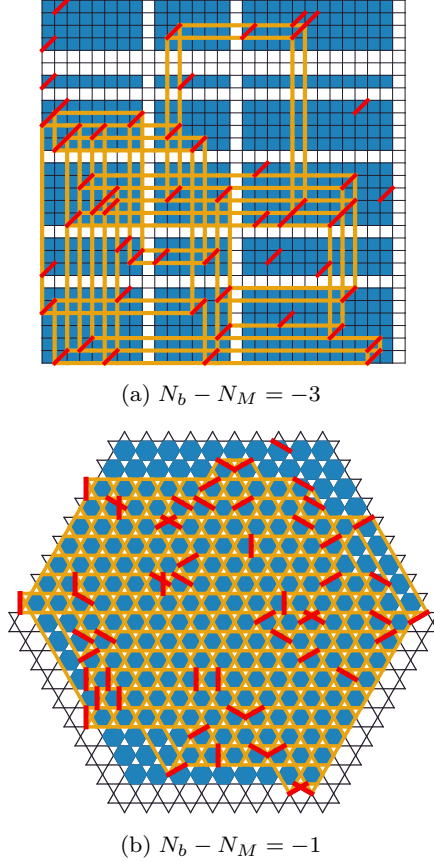


FIG. 8. (Color online) Snapshots of a regular square lattice (a) and a regular kagome lattices (b) using the conventions of Fig. 7. In contrast to the generic lattices, the regular square lattices (a) feature multiple rigid components of intermediate size, which are separated by lines of nonrigid regions, instead of one bulk rigid region. The regular kagome lattice (b) develops a large rigid component similar to the generic lattices but rigidifies much more slowly. A video of rigidity percolation in the square lattice is included as Supplemental Material [41].

distinct and equally likely coupon types, one asks how many coupons must be received before all  $n$  types have been seen at least once. This heuristic is in perfect agreement with the results of Ref. [17] asymptotically as  $L \rightarrow \infty$ ; we compare to numerical simulations in Fig. 3(a). We define the threshold probability  $p_r$  via  $\mathcal{P}_{\text{rigid}}(p_r) = \frac{1}{2}$ . In the limit  $L \rightarrow \infty$  we have

$$p_r^{\text{regular square}} = \ln L/L + \ln(2/\ln 2), \quad (3.4)$$

and clearly the right scaling variable for this transition is  $pL/\ln L$ , meaning that  $\mathcal{P}_{\text{rigid}}$  changes appreciably when  $p - p_r^{\text{regular square}} \sim \mathcal{O}(\ln L/L)$ .

We now postulate that, asymptotically, the regular kagome lattice in a hexagon becomes rigid precisely when every line meets at least one brace. One complication in repeating the above calculation is that the number of possible braces per “line” in the kagome lattice hexagon is not uniform, as the lines are of different length with our boundary conditions.

Thus let us first count the number of possible braces per line. There are three possible directions of lines: They lie at angles

$0, 2\pi/3, 4\pi/3$  relative to the  $+x$  axis, and we can further divide the set of lines with a given slope into two families which lie on opposite sides of the line cutting the hexagonal domain in half. These two families are related to each other by a reflection symmetry across that line.

We find that within one of these families, the line on the boundary admits  $l_1 = 3L + 1$  possible braces, and the other  $L - 1$  interior lines have length  $l_m = 4L + 4m - 3$  for  $m = 2$  to  $L$ . We multiply these counts by 6 because of the aforementioned sixfold symmetry.

Proceeding as we did for the square lattice:

$$\begin{aligned} \mathcal{P}_{\text{rigid}}(p) &= \prod_{i \text{ lines}} [1 - (1 - p)^{l_i}] \\ &\approx [1 - e^{-p(3L+1)}]^6 \prod_{m=2}^L [1 - e^{-p(4L+4m-3)}]^6 \\ &= [1 - e^{-p(3L+1)}]^6 e^{6 \sum_{m=2}^L (1 - e^{-p(4L+4m-3)})} \\ &\approx [1 - e^{-3pL}]^6 e^{\frac{3}{2p} [\text{Li}_2(e^{-8pL}) - \text{Li}_2(e^{-4pL})]}. \end{aligned} \quad (3.5)$$

In the last expression,  $\text{Li}_2(z) \equiv \sum_{k=1}^{\infty} \frac{z^k}{k^2}$  is the dilogarithm function, arising from approximating the sum as an integral. This expression compares well with the results from numerical simulations, depicted in Fig. 3(b), which *a posteriori* justifies our assumption above.

We now evaluate  $p_r^{\text{regular kagome}}$  in the limit  $L \rightarrow \infty$ :

$$\begin{aligned} \frac{1}{2} &\approx [1 - e^{-3p_r L}]^6 e^{\frac{3}{2p_r} [\text{Li}_2(e^{-8p_r L}) - \text{Li}_2(e^{-4p_r L})]} \\ -\ln 2 &\approx \frac{3}{2p_r} [-e^{-4p_r L}]. \end{aligned} \quad (3.6)$$

After taking the logarithm, we keep only the lowest powers of  $e^{-p_r L}$  in each factor. Physically, this corresponds to neglecting boundary effects and the variation in the line lengths and noticing that in the large- $L$  limit, the rigidity threshold is approached once the longest lines in the hexagon are coupled to the bulk:

$$\begin{aligned} \ln 2 &\approx \frac{3}{2p_r} e^{-4Lp_r} \\ p_r &= \frac{1}{4L} W\left(\frac{6L}{\ln 2}\right). \end{aligned} \quad (3.7)$$

The function  $W(\cdot)$  is the Lambert  $W$  function, defined to be the solution of  $x = W(x)e^{W(x)}$ . We find that the approximation above matches the solution in Eq. (3.6) to high accuracy only when  $L > 10^8$ . The asymptotic expansion for  $W(x)$  begins  $W(x) \sim \ln x - \ln \ln x$ , thus in the limit  $L \rightarrow \infty$ , we find that:

$$p_r^{\text{regular kagome}} \sim \frac{\ln L}{4L}. \quad (3.8)$$

The corrections to this do not go to zero but rather grow more slowly in  $L$  than  $\ln L/L$ . Regardless, this shows that the rigidity transition in the regular kagome hexagon resembles that of the regular square grid in that it occurs roughly after adding  $\mathcal{O}(L \ln L)$  braces.

Our calculation thus shows that  $\mathcal{P}_{\text{rigid}}(p)$  approaches a discontinuous jump as  $L \rightarrow \infty$ , which signals a first-order transition. On the other hand, one can extract a diverging length  $\xi^{\text{regular}} \sim 1/p$  near the transition, signaling a second-order

transition. Therefore this model relates to a group of interesting systems that exhibit such mixed nature [13,14,34–38].

### C. Number of floppy modes in regular lattices

The picture that follows from our assumptions and the calculation above is that, at large  $pL$ , the floppy modes of the regular lattice systems consist of one large coupled floppy mode and many isolated modes. This idea also allows us to calculate the number of floppy modes as the system approaches rigidity.

In the regular square grid, we expect that for large  $pL$ , the average number of floppy modes  $\langle F \rangle$  is the sum over all lines of the probability that the corresponding mode is not coupled to any others, i.e., that the line meets no braces. As each of the  $2L$  lines has length  $L$ , this predicts that

$$\langle F \rangle \rightarrow 2L(1-p)^L \approx 2Le^{-pL}. \quad (3.9)$$

In Appendix B, we exploit the mapping to the bipartite Erdős-Rényi model to derive the following expression for  $\langle F \rangle/L$  [Eq. (B18)] that is valid for all  $pL$ :

$$\frac{\langle F \rangle}{L} = 2[1 - s_*(pL)] \left\{ 1 - \frac{pL}{2}[1 - s_*(pL)] \right\}, \quad (3.10)$$

with  $s_*(pL)$  defined to be the stable solution of  $1 - s_* = e^{-pLs_*}$  [44]. In particular, this reduces to Eq. (3.9) in the limit  $pL \rightarrow \infty$ . Figure 4(a) compares Eqs. (3.9) and (3.10) to the results from numerical simulations.

Note that  $s_*$ , which is the probability that a given line mode is coupled to the “giant component” floppy mode (analogous to the magnetization in the Potts model [45], see also Appendix B), has a kink at  $pL = 1$  (see Fig. 15). For  $pL < 1$ ,  $s_*$  is identically 0, but then begins to grow linearly for  $pL > 1$ . This value of  $pL$  corresponds to the addition of only *half* of the braces required to get to  $N_M$ . The discontinuity in  $s_*$  leads to a discontinuity in the third derivative of  $\langle F \rangle/L$ , which is not visible in the plot of Fig. 4(a). This singularity corresponds to the formation of a giant component in the bipartite graph from the mapping. In rigidity terms, it is a transition where one floppy mode couples a large number of the row and column shear modes together, i.e., the formation of a “giant floppy mode.” From the mapping [or direct calculation from Eq. (3.10)], the critical exponents for this giant floppy mode transition are the same as for mean-field percolation [46].

For the regular kagome lattice, we observe a more dramatic transition at  $N_b = N_M$ . Figure 4(b) shows a kink in  $\langle F \rangle/L$  there, implying a discontinuity in the first derivative. Such a discontinuity can be interpreted in the following way. Equation (1.3) implies that this kink in  $F$  comes from a kink in the number of self-stresses. Since self-stresses occur when a bond is placed in a rigid region, this discontinuity implies a discontinuous jump in the density of rigid regions in the system [7]. Based on our numerical experiments, we observe that this corresponds to the formation of a *single* large rigid cluster in the bulk, as shown in Fig. 8(b).

Analytically, we have only been able to compute an asymptotic result for  $\langle F \rangle/L$  for large  $pL$ . As in our asymptotic form in Eq. (3.9), we expect that at large  $pL$  the expected number of floppy modes  $\langle F \rangle$  is the sum over all lines of the probabilities that each line meets no braces. We worked

out these probabilities in the previous section [though we computed the *product* of the *complementary* probabilities in Eq. (3.5)]. For large  $pL$ , we have

$$\begin{aligned} \langle F \rangle &= \sum_{i \in \text{lines}} (1-p)^{l_i} \\ &\approx 6e^{-pL} + 6 \sum_{m=2}^L e^{-p(4L+4m-3)} \\ &= 6e^{-4pL} + 6e^{-4p(L-1)} \frac{1 - e^{-4p(L-1)}}{1 - e^{-8p}} \\ &\approx 3Le^{-4pL} \frac{1 - e^{-4pL}}{2pL}. \end{aligned} \quad (3.11)$$

We find that this matches well the numerical results as soon as  $N_b > N_M$ , depicted in Fig. 4(b).

One important fact which is apparent in the above analysis is that in both the regular square and regular kagome systems, the number of floppy modes remains “extensive,” i.e., in sufficiently large systems,  $\langle F \rangle$  scales with the linear system size  $L$ , for all  $N_b/N_M$ . We shall see in the next sections that this is not true in the generic systems once the bulk rigidifies.

## IV. THEORY OF RIGIDITY PERCOLATION ON GENERIC ISOSTATIC LATTICES

### A. Formation of rigid regions

In this section we develop an analytical theory to predict where and how rigidity develops as braces are randomly added to the system. We focus on the generic square lattice, with results that are readily extended to the kagome lattice. As we will see, added braces pose independent constraints on the system’s floppy modes until close to the Maxwell point, when a single brace makes the entire bulk of the system rigid (see Fig. 7). Once the bulk is rigid, only the edges can contain floppy modes, and these edge modes may persist well above the Maxwell point.

Rigidity percolation on the generic square lattice differs from that of the regular square lattices in an important way. It is worth noting that the bipartite graph mapping for the regular square lattice does not preserve any information on the distances between rows and columns. For example, if three braces join row  $\mathcal{R}_i$  with column  $\mathcal{C}_k$ , row  $\mathcal{R}_i$  with column  $\mathcal{C}_l$ , and  $\mathcal{R}_j$  with column  $\mathcal{C}_k$ , then  $\mathcal{R}_i, \mathcal{R}_j, \mathcal{C}_k, \mathcal{C}_l$  already belong to the same rigid cluster, and the addition of a brace at the plaquette of  $\mathcal{C}_l$  and  $\mathcal{R}_j$  must be redundant, no matter how far the distance is between  $\mathcal{R}_i$  and  $\mathcal{R}_j$  and  $\mathcal{C}_k$  and  $\mathcal{C}_l$ . For a generic square lattice, in contrast, such a fourth brace is only redundant if  $\mathcal{R}_i$  and  $\mathcal{R}_j$  are neighboring rows and  $\mathcal{C}_k$  and  $\mathcal{C}_l$  are neighboring columns, because no straight lines exist to directly transmit stress to infinite distance. Thus, as shown in Fig. 9, if a generic square lattice is rigid, the corresponding regular square lattice with the same configuration of braces must also be rigid, but the converse is not true. In the following, we show that due to the difference discussed above, the generic square lattice does not have any states of self-stress until the bulk of the lattice is already rigid.

Consider Region I, a rectangular region with length  $l$  greater than or equal to its width  $w$ , as depicted in Fig. 10. The

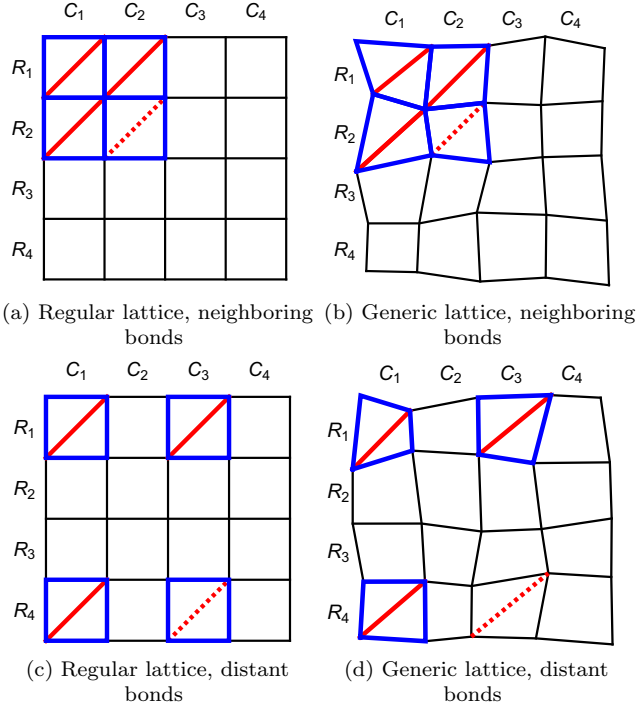


FIG. 9. (Color online) Regular and generic lattices differ dramatically in how individual plaquettes become rigid. As shown in (a) and (b), in either type of lattice three braced plaquettes render the fourth plaquette that shares a vertex with them rigid. Because the floppy modes of the regular lattice shear whole columns or rows, three braced plaquettes can also render a fourth distant plaquette rigid, meaning that an additional brace placed there would generate a self-stress. In (c), the plaquette with the dashed line is rigid because shearing it would require rotating the plaquettes at  $(R_4, C_1)$  and  $(R_1, C_3)$  to different angles, which would then shear the braced plaquette at  $(R_1, C_1)$ . In contrast, the generic mixing of floppy modes in (d) means that the trio of braced plaquettes do not render  $(R_4, C_3)$  rigid, and so that when a brace is placed there it eliminates a floppy mode, rather than generating a self-stress as in the equivalent regular lattice.

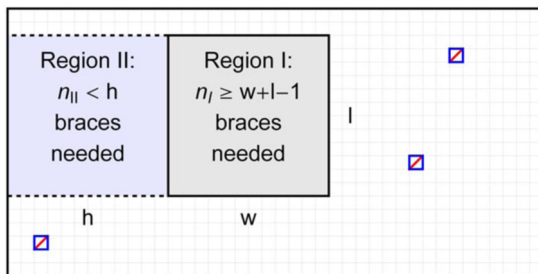


FIG. 10. (Color online) Consider the possibility of Region I, measuring  $l$  by  $w$  plaquettes, becoming an isolated rigid region in a large generic square lattice. This would require  $l + w - 1$  independent braces in Region I. However, Region II would then experience  $l - 1$  constraints from its shared edge with Region I and so would require only  $h$  additional independent braces placed in its interior to be made rigid. For large systems, this occurs with finite probability only for  $h \sim \mathcal{O}(1)$ . Thus, as discussed in the text, rigid regions first form with nearly  $N_M = 2L - 3$  braces, and such regions span the entire system except possibly for a few rows and columns near the edge.

region, including bonds and vertices on its boundaries but not bonds connecting this region to neighboring vertices, has  $2(l + 1)(w + 1)$  degrees of freedom and  $2lw + l + w$  constraints, so  $w + l - 1$  independent braces are needed to eliminate the floppy modes of Region I. We now ask what the probability is that Region I is an *isolated* rigid region. Since braces in the generic lattice cannot render distant plaquettes rigid except by also rendering intervening ones rigid as well, only braces within Region I itself can contribute to it becoming an isolated rigid region. Thus, a necessary condition for Region I to be rigid and isolated is that it contain at least  $w + l - 1$  braces, which it does with probability

$$\sum_{j=w+l-1}^{wl} \binom{wl}{j} p^j (1-p)^{wl-j}, \quad (4.1)$$

where  $p = N_b/(L - 1)^2$  is the probability of a brace being placed on a plaquette and  $\binom{wl}{j}$  is a binomial coefficient.

For  $w = l = 2$ , this probability is  $\mathcal{O}(p^3)$ , with larger regions higher order in  $p$ . As we will see, the bulk of the system becomes rigid near the Maxwell point, when  $p \sim 1/L$ , so the probability of a small isolated region occurring *anywhere* in the system is only  $\mathcal{O}(L^{-1})$  and vanishes for large systems. The one exception,  $2 \times 1$  regions, occur with finite frequency but at least three braces are required to render another plaquette rigid. This nonexistence of small rigid regions is confirmed by simulation results and permits the use of Maxwell counting in much of our analysis.

In contrast to small regions, larger ones require a lower density of braces  $(w + l - 1)/wl$  and have more ways to distribute those braces, generating a large combinatorial factor in Eq. (4.1). This suggests that large rigid regions become possible before small ones and, indeed, when  $l$  is large, the central limit theorem applies, and the probability of having exactly  $j$  braces in Region I becomes

$$\frac{1}{\sqrt{2\pi wlp(1-p)}} \exp\left[-\frac{(j - wlp)^2}{2wlp(1-p)}\right], \quad (4.2)$$

so as  $p$  approaches  $(w + l - 1)/(wl)$  Region I may become rigid. This occurs first for the largest regions, so it is clear already that the first rigid region to appear will cover much of the system. However, for Region I to be not only rigid but also isolated Region II must remain floppy.

When Region I is rigid, a single brace in the right column of Region II renders that entire column rigid. Such a braced plaquette, along with the rigid plaquettes of Region I immediately to its right, would mean that the plaquette above (or below) it would be fully constrained and rigid. Thus, because of the rigid edge this column, which would otherwise have  $l$  degrees of freedom, has only one. Because of this, once Region I is rigid Region II needs only an additional  $h$  independent braces, rather than  $l + h - 1$ , to be rigid as well.

On average, Region II contains at least  $2h$  braces, twice as many as would make it rigid, with a standard deviation in its brace number proportionate to  $\sqrt{h}$ . Thus, when Region I is rigid Region II contains sufficient braces to make it rigid as well *unless* possibly its width  $h$  is  $\mathcal{O}(1)$ . Thus, when rigid regions appear at or near the Maxwell point they fill the entire system with the possible exception of a few rows and columns

on the edges. Indeed, as depicted in Fig. 7, as braces are added in simulation no rigid regions form until a *single brace* renders the bulk of the system rigid, leaving only a small, random number of floppy rows or columns on the edges of the system in a first-order-like transition. We say then that the system has a rigid bulk, and we now characterize its edge modes.

### B. Edge modes

We now develop a theory to describe the number of floppy modes, which we call *edge modes*, that are present on an edge when the bulk is rigid. We say that the  $m$  columns on the edge of a system have *minimal edge rigidity* if the braces present in them would render them rigid but unstressed if the rest of the system were rigid. Consider the first column along the left edge of the system. If the columns to its right were rigid then a single brace would make the entire column rigid since a rigid plaquette combined with two from the rigid region to the right will also make the plaquettes above and below it rigid, as in Fig. 9(b). The column has  $L - 1$  plaquettes that can be sheared, but the  $L - 2$  vertices (not counting those on the edge of the system) it shares with the rigid region couple the plaquette modes together, so there is only one independent floppy mode associated with this column. A single random brace gives the first column minimal edge rigidity. Similarly, the first two columns could be given minimal edge rigidity if two braces were placed in the first column or if one were placed in both of the first two columns. On the other hand, if two braces were placed in the second column and zero in the first, then the second column could be stressed (if the third column were already rigid) while the first would necessarily remain floppy. In general, minimal edge rigidity requires that the  $m$  columns contain exactly  $m$  braces and that there is no set of them connected to the bulk that contains more braces than columns. That is,  $m$  columns on the edge have minimal edge rigidity if they contain  $m$  braces distributed so

$$\sum_{k=m-j+1}^m n_k \leq j \quad \text{for all } j = 1, 2, \dots, m, \quad (4.3)$$

where  $n_i$  is the number of braces in the  $i^{\text{th}}$  column.

Consider a column such as column four in Fig. 11. Adding a single brace to that column would give the first four columns minimal edge rigidity, so we say that that the column *contains an edge mode*. If we also added a brace to the sixth column, that would give the first six columns minimal edge rigidity, so we say that it, too, contains an edge mode. Generally, the requirement for an edge mode to be contained in the  $m^{\text{th}}$  column counting inward either from the edge or from another column with a floppy edge mode is for the relations of Eq. (4.3) to be satisfied with strict inequality. That is, the column containing the edge mode must have zero random braces, it and its left neighbor combined have one or fewer, and so on. When the bulk is rigid, the number of floppy modes associated with an edge is equal to the number of columns containing floppy edge modes as defined this way. When the bulk is not rigid, the true number of floppy modes is generally greater, since rigid regions encourage rigidity around them, as discussed above.

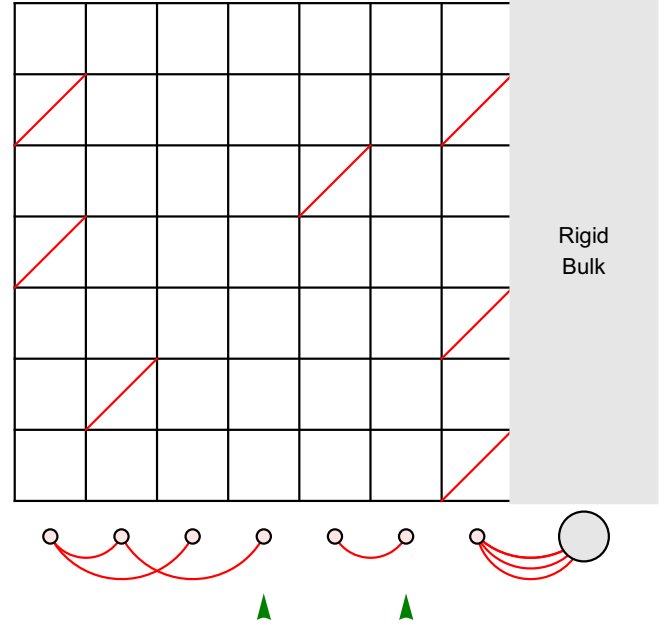


FIG. 11. (Color online) A floppy region on the left edge of a generic square lattice with a rigid bulk. For visual clarity, we show only a few rows and do not depict the generic displacements of vertices. There are seven random braces in seven columns, but because of their distribution, the edge is not rigid. Counting from the outer edge and treating each column as a single vertex in a graph, a brace in a column links it to the next column not already part of the rigid cluster or to the bulk, as depicted in the graph below the main diagram. Because the fourth and sixth columns would require additional braces to connect the edge to the bulk, these two columns are said to contain *edge modes*, indicated by green arrowheads. These two modes make the first six columns floppy, while the seventh has become part of the rigid bulk. As discussed in the text, these edge modes play an important role in the onset of rigidity.

We now wish to determine the statistics of these edge modes. The probability,  $\mathcal{P}_m$ , that the  $m^{\text{th}}$  column contains the first edge mode is simply the probability that the first  $m - 1$  columns are minimally rigid and the  $m^{\text{th}}$  column itself has no random braces. For a fixed number of random braces, this is simply the fraction of configuration of  $N_b$  braces to the left and right of the  $m^{\text{th}}$  column consistent with this condition, which can be expressed in terms of combinatorial factors as

$$\mathcal{P}_m = \frac{\binom{(L-1)(L-m-1)}{N_b-m+1} \binom{(L-1)m}{m-1}}{\binom{(L-1)^2}{N_b}} \times \sum_{\{n_i\}_{i=1}^m} \prod_{i=1}^m \binom{(L-1)}{n_i}, \quad (4.4)$$

where the sum is over only those brace configuration  $\{n_i\}_{i=1}^m$  consistent with an edge mode being present in the  $m^{\text{th}}$  column. For large systems the number of braces per column follows a Poisson distribution with a mean value  $c \equiv N_b/(L - 1)$  braces

per column, so

$$\mathcal{P}_m = e^{-mc} c^{m-1} \sum_{\{n_i\}_{i=1}^m} \prod_{i=1}^m \frac{1}{n_i!}. \quad (4.5)$$

One can add a brace to any of  $m$  columns in order to make the edge mode minimally rigid, so the combinatorial factor is  $m^{-1}$  times the equivalent for a minimally rigid set of braces. The minimally rigid set of braces on  $m$  columns can be mapped onto the set of spanning trees of a graph of  $m$  distinguishable edges by noting that, counting from the edge, each brace connects the column it is in to the first column that is not already in the rigid cluster (see Fig. 11). Thus, applying Cayley's formula for the number of spanning trees of a complete graph [47],

$$\mathcal{P}_m = e^{-mc} c^{m-1} \frac{m^{(m-2)}}{(m-1)!}. \quad (4.6)$$

$\mathcal{P}_m$  is only physically meaningful when the rigid bulk is present, near or above  $N_b = N_M$ . Then  $\mathcal{P}_m$  quickly falls as  $m$  increases, and even in large systems only a few columns at each edge are potentially floppy. Then the probability  $R$  that the edge will be rigid when the bulk is rigid is

$$R = 1 - \sum_{m=1}^L \mathcal{P}_m(N_b), \quad (4.7)$$

where the sum quickly converges for  $N_b \gtrsim N_M/2$ , so columns far from the edge do not contain edge modes.

Thus far, we have considered only the *first* edge mode on an edge. However, an edge may contain two or more modes, as in Fig. 11. Once the first edge mode has been identified, the conditions under which a second appears  $m$  columns inward are simply those of Eq. (4.3), applied to the  $m$  columns to the right of the first edge mode rather than to the first  $m$  columns counting from the outer edge. Thus, an edge contains  $N_{em}$  edge modes with probability  $R(1-R)^{N_{em}}$  and

$$\langle N_{em} \rangle = \frac{1-R}{R}. \quad (4.8)$$

Although we have relied on the concept of a rigid bulk to describe these edge modes, it is the edge modes themselves that determine when the bulk becomes rigid. Consider a system with a total number of edge modes  $\sum N_{em}$  which leave  $N_{col}$  columns and rows floppy. Since the floppy edges do not support states of self-stress, Maxwell counting indicates that they contain  $N_{col} - \sum N_{em}$  random braces and that the remaining bulk comprises an area originally containing  $N_M - N_{col}$  floppy degrees of freedom. This leads to the criterion for bulk rigidity,

$$N_M - N_b \leq \sum_{\text{edges}} N_{em}. \quad (4.9)$$

That is, the bulk is rigid even below the Maxwell point so long as the needed floppy modes can all be found at the edge. The bulk is always rigid above the Maxwell point, since no states of self-stress occur without a rigid bulk. When the bulk first becomes rigid the above relationship is satisfied with equality. Since even in large systems only a few edge modes occur with substantial probability the bulk becomes rigid either at the Maxwell point or only a few braces below. This is a first-order transition in which a single brace makes all but perhaps  $\mathcal{O}(L)$

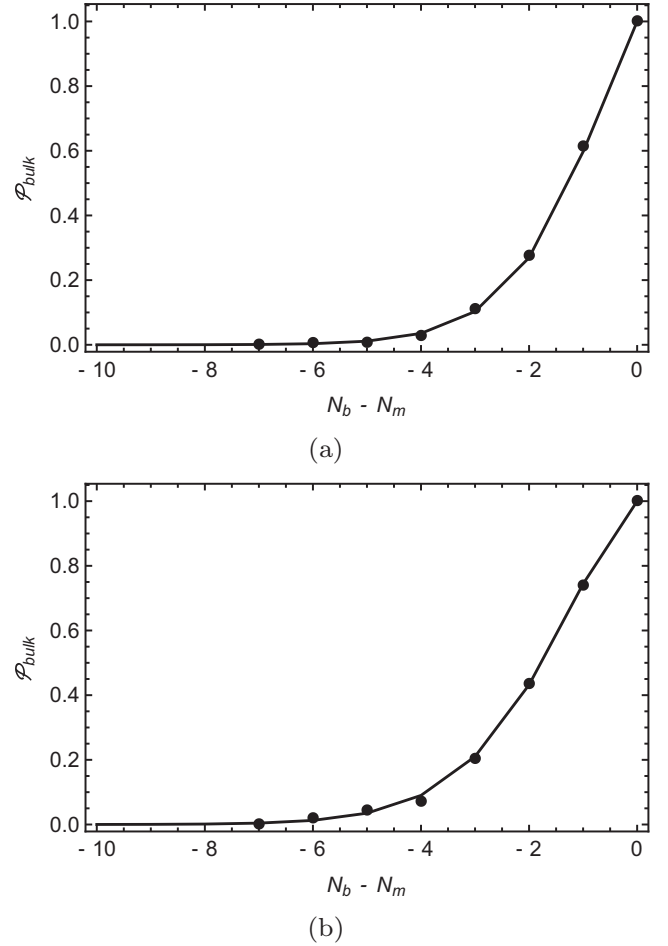


FIG. 12. The bulk rigidity probability as a function of  $N_b - N_M$  on (a) generic square lattices with linear size  $L = 200$  and (b) generic kagome lattices with  $L = 100$ . The solid lines are theoretical results of Eq. (4.9) in the large-system limit. The dots are simulation results. Error bars are smaller than the symbols.

plaquettes rigid. Then, as additional braces are added to the system, each one either eliminates an edge mode or generates a state of self-stress within the bulk.

### C. Rigidity statistics

The probability  $\mathcal{P}_{\text{bulk}}$  that the bulk of the system is rigid is simply the probability that the condition of Eq. (4.9) is met:

$$\mathcal{P}_{\text{bulk}}(N_b) = 1 - \Pr \left( \sum_{\text{edges}} N_{em} < N_M - N_b \right). \quad (4.10)$$

For large systems, the corners where row and column modes meet are negligible and the statistics of the modes on different edges follow independently from Eq. (4.6). This probability  $\mathcal{P}_{\text{bulk}}$  is plotted in Fig. 12, in quantitative agreement with simulation.

This bulk rigidity probability also determines the mean number of floppy modes present. When the bulk is not rigid, the number of floppy modes follows from Maxwell counting. When, on the other hand, the bulk is rigid the edge modes of

Eq. (4.8) are the only modes present so generally

$$\langle F \rangle = (1 - \mathcal{P}_{\text{bulk}})(N_M - N_b) + \mathcal{P}_{\text{bulk}} \frac{4R}{1 - R}. \quad (4.11)$$

Well below the Maxwell point each brace eliminates a floppy mode, as indicated by the first term. At or above  $N_M$ , only the edge modes from the second term are present. Slightly below the Maxwell point the system may or may not have a rigid bulk, and both edge modes and bulk floppy modes contribute to different lattice realizations seen in simulation.

Separately from the rigidity of the bulk, there is the probability  $\mathcal{P}_{\text{rigid}}$  that the system is entirely rigid, without even edge modes. This can occur only for  $N_b \geq N_M$  and requires simply that all four edges be rigid as described in Eq. (4.7).

Thus,

$$\mathcal{P}_{\text{rigid}} = \begin{cases} 0 & \text{for } N_b < N_M \\ R^4 & \text{for } N_b \geq N_M \end{cases}. \quad (4.12)$$

At the Maxwell point, this has finite probability  $\approx 0.403$ , the probability that no edge modes are present. Unlike bulk rigidity, which is achieved within a few braces of the Maxwell point, total rigidity generally requires  $\mathcal{O}(L)$  additional braces, since each brace is much more likely to fall in the bulk than to eliminate an edge mode.

The picture we have developed is for the generic square lattice but applies without substantial modification to the generic kagome lattice with a hexagonal geometry. For the kagome, there are six edges and three principal directions, but the edge modes on each edge are eliminated by random braces in much the same way as the square lattice. Unlike the square lattice, where every column has  $L - 1$  sites to place random braces, the  $m^{\text{th}}$  “column” from an edge in the kagome lattice has  $L + m - 2$  sites, but since only the first few columns can contain edge modes this does not affect the behavior of large systems.

This analytic theory of edge modes thus predicts the probability of the rigid bulk, the probability of total rigidity, and the average number of floppy modes, as shown, respectively, in Figs. 12, 5, and 6. Using no free parameters, it achieves quantitative agreement with the behavior of the simulations of generic square and kagome lattices below, above, and precisely at the rigidity transition.

Were we instead to work in an ensemble with fixed brace probability  $p$ ,  $N_b$  would become a random variable with, to leading order for large lattices, mean  $pL^2$  and standard deviation  $L\sqrt{p}$ . This would lead to a rigidity transition at  $p_r = 2/L$  in which number fluctuations would smooth out the transition that otherwise occurs via a single brace to one that takes place over a range of probabilities  $\Delta p \sim L^{-3/2}$ .

## V. CONCLUSION AND DISCUSSION

We have elucidated the rich phenomenology of rigidity transitions in regular and generic isostatic lattices with  $N_b$  added braces. We now summarize our main findings.

Regular lattices become rigid after approximately  $\mathcal{O}(L \ln L)$  braces are added, in accordance with “coupon-collector” heuristics. However, they first undergo a transition at  $\mathcal{O}(L)$ . In the regular square lattice, this transition is weak and has a discontinuity in the third derivative of the average

number of floppy modes  $\langle F \rangle$ . The regular kagome lattice appears to form a giant rigid cluster at  $\mathcal{O}(L)$  via a first-order transition— $\langle F \rangle/L$  then decays exponentially in  $N_b - N_M$  until the rigidity transition occurs.

In generic lattices, the nature of the rigidity transition differs markedly. No extended rigid regions exist in such a lattice until a single brace renders the entire bulk of the system rigid at or a few braces before the Maxwell point. Once the bulk is rigid, floppy edge modes may exist and persist well above the Maxwell point even as self-stresses proliferate in the bulk.

In both types of systems, despite the fact that the rigidity transitions are first order, the transition probabilities scale as  $1/L$  (to lowest order). This determines at fixed  $p$  a critical system size which diverges like  $1/p$ .

Below we point out some connections between the bracing percolation problem to other work and suggest some directions for future work.

A previous study of braced generic square lattices [20] attached the system to rigid bars along diagonals, preventing the appearance of edge zero modes and thereby altering the nature of the transition. How, then, do the boundary conditions and the shape of the boundary influence the edge modes and the rigidity transition? It is pointed out in Ref. [24] that lattices near the isostatic point are very sensitive to boundary conditions, as the number of floppy modes are often subextensive. Systems with fixed boundaries may experience *edge self-stresses* which control the nature and location of their rigidity transition, just as the *edge zero modes* do in the system with free boundary conditions that we consider presently.

The transition we observe appears to be very closely related to the rigidity transition on the Erdős-Rényi model on the complete graph [7–10]. Just as in our braced isostatic lattices, the systems exhibit the sudden appearance of a giant rigid cluster when the number of edges is  $\mathcal{O}(1/N)$ . Our arguments for the nonexistence of small rigid clusters in Sec. IV A are similar to those made in Refs. [8,48] and likely can be made rigorous along similar lines. Several authors [7,10] have considered the problem of rigidity percolation on complete graphs with an additional “applied field” of random additional pin and slider constraints to a fixed background and have found true critical and tricritical behavior in the formation of a giant rigid cluster. It would be interesting to see whether addition of such constraints also induce similar phenomena in the bracing percolation problem.

In this paper we took the point of view of changing the density of braces while fixing the system size. One can also frame the results by instead imagining what happens if the density of braces is fixed and the system size is changed. In particular, one could imagine cutting out from a large system a sample with linear size  $L$  and considering the rigidity properties of this sample. From our results, we see that for generic systems, provided that  $L$  is sufficiently small so  $N_b \leq N_M$ , the system consists of many small rigid regions, and when  $L$  is large enough that  $N_b \geq N_M$ , the bulk of the system rigidifies. In Ref. [49], the authors consider networks arising from jammed packings and use the system size  $L$  at which the bulk of the system rigidifies to *define* a rigidity length scale  $l^*$ . In our system,  $l^* \sim \mathcal{O}[(N_B/N_M)^{-1}]$ , perfectly analogous to their result in which  $l^*$  diverges as  $\mathcal{O}(\delta z^{-1})$ .

Indeed, the rigidity transition in generic isostatic lattices shares several interesting similarities with the jamming transition of frictionless spheres which occurs at the Maxwell point as well [13]. As next-nearest-neighbor braces are randomly added, *generic isostatic lattices display no self-stress until a compact rigid bulk occurs very close to the Maxwell point, and the addition of one more brace from this point renders the system globally stressed*. This is strikingly similar to the phenomena in jamming as reported in Ref. [50]. In addition, our density argument for the first-order-like transition in Sec. IV A agrees with the counting in the cutting argument from Ref. [51]. Generic isostatic lattices are then closer to contact networks of jammed packings than either regular isostatic lattices or diluted generic triangular lattices, because the latter two can develop *self-stresses* before rigidity percolation.

The elastic moduli are additional quantities that can be compared with jamming. Systems of frictionless spheres display a discontinuous jump in bulk modulus at jamming, whereas shear modulus grows with  $(\Delta z)^1$ . A recent paper by Stenull and Lubensky [52] pointed out that generic versions of Penrose tilings show the same elastic moduli as jammed packings at point J. Thus, it will also be interesting to explore the rigidity transition as bonds are randomly added and removed from the generic Penrose tilings.

Bootstrap percolation/ $k$ -core percolation [14,36,37] and kinetically constrained models [38] are other combinatorial models on graphs which have been used to study jamming transitions. They have some similar features; in the closest-related lattice bootstrap percolation models, where lattice sites are deemed active with fixed probability [36,37], as the system size grows the critical occupation probability goes to zero. In those models, this has been interpreted as a kind of metastability—the idea being that there is a size above which the system is likely to contain a “critical droplet” which causes the entire system to be jammed [36]. In a  $k$ -core problem on the Bethe lattice, a mixed first-and-second-order transition was observed, with the fraction of sites in the spanning cluster undergoing a discontinuous jump followed by critical scaling [14].

The mechanism of rigidity percolation in generic braced isostatic lattices has some features of both of these transitions. In the systems we study, the critical length scale arises from the difference in the scaling with system size between the number of floppy modes coming from the free boundary and the number of added braces when the density is held fixed. Nonetheless, there may still be some metastability phenomena. If braces are added at random until the system becomes rigid and then removed at random one by one, then due to the random distribution of self-stresses, the system is likely to lose rigidity with a different number of braces than that with which it gained rigidity. However, our results show that the width of this metastability window should be quite small, approximately  $\mathcal{O}(1)$  in the generic systems. We do not observe critical exponents above the first-order-like jump above  $p_r$  in our systems, as in the  $k$ -core problem of Ref. [14]; however, we can identify a diverging length scale from the system size dependence of  $p_r \sim 1/L$ . The connections between bootstrap and  $k$ -core percolation models and bracing percolation deserve to be further studied. One can also ask whether braced isostatic

systems exhibit “jamming by shape” as some kinetically constrained models do [53].

Because one can continuously tune a lattice between regular and generic by small perturbations of lattice sites positions, it will be interesting to examine how some floppy modes in the regular isostatic lattices are lifted to finite energy, whereas some keep being floppy modes, as well as how modes crossover from extended to localized.

For the generic bracing percolation systems we consider, the shape distribution of the eventual giant rigid cluster can be computed fairly easily because rigid clusters must be either rectangular or hexagonal. It would be interesting to compare this to the average shape of the typical large rigid cluster in the jammed packings of Ref. [49]. While the rigid clusters seem to have a simple shape, the plots in Fig. 7 suggest questions about the distribution and size of *stressed* regions (yellow bonds). The stressed regions have significance for the robustness of the systems, as they consist of the bonds that can be removed without making the system floppy.

## ACKNOWLEDGMENTS

B.G.C. thanks Louis Theran for illuminating discussions. B.G.C. was supported by NSF Grant No. DMR05-47230 as well as by the Foundation for Fundamental Research on Matter (FOM), which is part of the Netherlands Organisation for Scientific Research (NWO).

## APPENDIX A: BRACED RIGIDITY MATRIX FOR THE BRACED REGULAR KAGOME LATTICE

In this Appendix, we derive a simplified rigidity matrix for next-nearest-neighbor bonds on the regular kagome lattice, which we call the braced rigidity matrix. This matrix representation is used in the rank calculations in the numerical results of Sec. II.

The usual rigidity matrix keeps track of all  $2N$  possible displacements of the  $N$  points in a spring network and each row of the matrix expresses how these displacements are coupled to each other by each spring in the system. The rigidity matrix thus is  $N_c \times 2N$ .

The braced rigidity matrix instead uses only the degrees of freedom that a regular kagome lattice allows (arising from modes localized on three families of lines, see Fig. 13). We now consider how each brace couples these degrees of freedom together.

The three families of lines are at angles of  $0$ ,  $2\pi/3$ , and  $4\pi/3$  relative to the  $x$  axis. The floppy mode localized on a horizontal straight line  $l$  in the kagome lattice has an infinitesimal displacement on each vertex equal to  $(\frac{\sqrt{3}}{2}, \pm \frac{1}{2})$  (with the signs alternating and chosen so the displacement at a vertex is always perpendicular to the nonhorizontal line intersecting  $l$  there). Other line-localized modes can be generated similarly.

We now introduce some notation. We denote the  $2N$ -dimensional vectors corresponding to the modes supported on lines in these directions as  $v_{0,i}$ ,  $v_{0,j}$ , and  $v_{0,k}$ , respectively, where the indices  $i, j, k$  label the specific line with the angle specified by the first index. Note that for a hexagonal system, there are  $2L$  lines running in each direction. It is

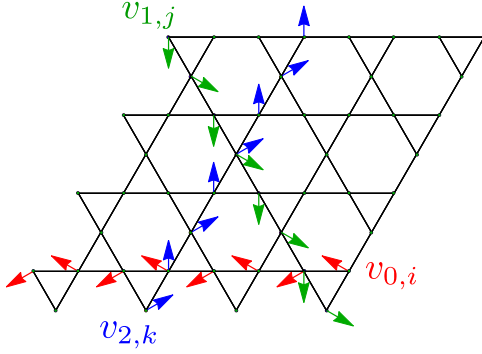


FIG. 13. (Color online) Three line modes in a portion of the regular kagome lattice. The line modes supported on horizontal lines (red) are denoted  $v_{0,i}$ , those on lines with angle  $2\pi/3$  (green) are denoted  $v_{1,j}$  and those on lines with angle  $4\pi/3$  (blue) are denoted  $v_{2,k}$ . On a hexagon, the indices  $i, j, k$  run from 1 to  $2L$ .

straightforward to check that the  $6L$  modes  $v_{0,i}, v_{1,j}, v_{2,k}$  span the space of zero modes (floppy modes as well as translations and rotations) of the regular kagome hexagon with no braces.

Now consider a brace coupling the motions of two particles. The constraint imposed by requiring this brace not to stretch to linear order is that the difference in displacements of the two particles must be perpendicular to the direction of the bond. Since each particle is at the intersection of two lines, there are only two modes which contribute to the motion of any particle. Thus there are four line modes which are constrained by the brace, which are always in a configuration like that in Fig. 14 or some rotation thereof. Let us suppose these four modes are  $v_{0,i}, v_{0,i+1}, v_{1,j}$ , and  $v_{2,k}$ . If the coefficients of these four modes in some motion are  $c_{0,i}, c_{0,i+1}, c_{1,j}$ , and  $c_{2,k}$  then the brace is unstretched if the  $y$  component of the velocity at the upper particle is equal to the  $y$  component of the velocity at the lower particle:

$$-c_{0,i} - 2c_{1,j} = c_{0,i+1} + 2c_{2,k} \quad (\text{A1})$$

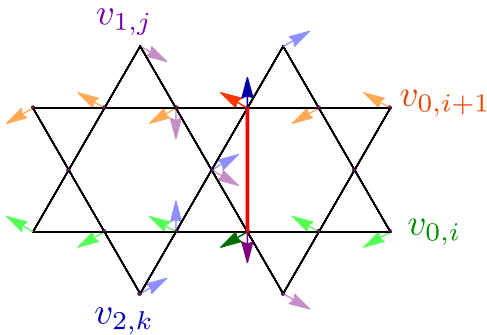


FIG. 14. (Color online) The constraint from a brace (red) on the coefficients of four line modes  $v_{0,i}$  (green),  $v_{0,i+1}$  (orange),  $v_{1,j}$  (purple), and  $v_{2,k}$  (blue). Suppose that the coefficients are  $c_{0,i}, c_{0,i+1}, c_{1,j}, c_{2,k}$ . Then the brace is unstretched if the  $y$  component of the velocity at the upper particle is equal to the  $y$  component of the velocity at the lower particle: thus  $-c_{0,i} - 2c_{1,j} = c_{0,i+1} + 2c_{2,k}$ , or, equivalently,  $c_{0,i} + c_{0,i+1} + 2c_{1,j} + 2c_{2,k} = 0$ .

or, equivalently,

$$c_{0,i} + c_{0,i+1} + 2c_{1,j} + 2c_{2,k} = 0. \quad (\text{A2})$$

We have identical linear equations for the other braces, though the indices differ. Note that all of these have integer coefficients. We combine these equations together for every brace and the resulting integer matrix is  $N_b$  by  $6L$ . This is the braced rigidity matrix.

## APPENDIX B: FLOPPY MODES OF THE REGULAR SQUARE LATTICE

In this Appendix, we compute the number of floppy modes of the randomly braced regular square lattice. This is done by exploiting the map to a random bipartite graph model (described in Sec. III, see also Fig. 2) and adapting the results of Engel *et al.* [44], who use the Fortuin-Kasteleyn cluster expansion to write the expected number of connected components with a certain  $q$ -weighted distribution as the  $q \rightarrow 1$  limit of the magnetization in a Potts model.

The complete bipartite graph  $K_{L,L}$  is the graph with two partitions of  $L$  vertices  $P_1, P_2$ , such that every vertex in  $P_1$  is adjacent to every vertex in  $P_2$  (and vice versa) but is not adjacent to any vertex in  $P_1$ , and, similarly, vertices in  $P_2$  are not adjacent to any vertices in  $P_2$ . Note that for notational simplicity in this section we work with a  $(L+1) \times (L+1)$  square grid, so the vertices in  $P_1$  correspond to the  $L$  adjacent pairs of rows, and the vertices in  $P_2$  correspond to the  $L$  adjacent pairs of columns.

Let  $G(K_{L,L}, \gamma)$  be a random graph on the set of vertices of  $K_{L,L}$  where each of the  $L^2$  edges of  $K_{L,L}$  is present with probability  $p = \gamma/L$ , independently. This gives a bipartite Erdős-Rényi-type model. Engel *et al.* related the Erdős-Rényi model on the (ordinary) complete graph to the Potts model by studying a probability distribution on random graphs which is *biased* towards having either more or fewer connected components depending on a new parameter  $q$ . Taking the limit  $q \rightarrow 1$  yields results relevant for the unbiased distribution. Below we adapt their work to  $K_{L,L}$ .

We first define the Potts model on this graph. Each vertex of  $K_{L,L}$  carries a spin variable  $\sigma_i$  which can take any of  $q$  values, that is,  $\sigma = 0, 1, \dots, q-1$ . For later convenience, the spin variables on vertices in  $P_1$  will be called  $\sigma_i$  for  $i = 1$  to  $L$  and the spin variables on vertices in  $P_2$  will be called  $\tau_j$  for  $j = 1$  to  $L$ . The energy function of a spin configuration (at zero field, which suffices for our purposes in this section) is then

$$E(\{\sigma_i, \tau_j\}) = -\frac{1}{2L} \sum_{i=1}^L \sum_{j=1}^L \sigma_i \tau_j. \quad (\text{B1})$$

The partition function is

$$\mathcal{Z}(\beta, q, L) = \sum_{\{\sigma_i, \tau_j\}} \exp[-\beta E(\{\sigma_i, \tau_j\})], \quad (\text{B2})$$

where we sum over all  $q^{2L}$  possible spin configurations. The free energy (per site) in the thermodynamic limit ( $L \rightarrow \infty$ ) is

$$f(\beta, q) = -\lim_{L \rightarrow \infty} \frac{1}{2\beta L} \ln \mathcal{Z}(\beta, q, L). \quad (\text{B3})$$

If  $c(\gamma)$  is the typical number of components per vertex in a graph in the Erdős-Rényi model on  $K_{L,L}$  with parameter  $p = \gamma/L$ , then to leading order in  $L$ , the results of Ref. [44] show that

$$c(\gamma) = (2\gamma) \left. \frac{\partial f(2\gamma, q)}{\partial q} \right|_{q=1}. \quad (\text{B4})$$

We may calculate the free energy of the Potts model on  $K_{L,L}$  using a mean-field ansatz, see, e.g., Ref. [54]. We begin by introducing the following  $2q$  order parameters (“magnetizations” of each type of spin in  $P_1$  and  $P_2$ ):

$$m_k = \frac{1}{L} \sum_{i=1}^L \delta(\sigma_i, k), \quad (\text{B5})$$

$$n_k = \frac{1}{L} \sum_{j=1}^L \delta(\tau_j, k). \quad (\text{B6})$$

Thus  $m_k$  is the fraction of spins in  $P_1$  which are in spin state  $k$  for  $k = 0, 1, \dots, q-1$ , and, similarly,  $n_k$  is the fraction of spins in  $P_2$  in state  $k$  and hence  $\sum_k m_k = \sum_k n_k = 1$ . In terms of these variables (and neglecting fluctuations), our energy function  $E(\cdot)$  becomes

$$E(\{m_k, n_k\}) = -\frac{N}{2} \sum_{k=0}^{q-1} m_k n_k. \quad (\text{B7})$$

It turns out that we get a simplification here because the sizes of  $P_1$  and  $P_2$  are the same. In particular, we shall see that the free energy is very nearly the same as that of the usual mean-field Potts model on a complete graph.

In going from the microscopic variables  $\{\sigma_i, \tau_j\}$  to the macroscopic variables  $\{m_k, n_k\}$  we get an entropy of mixing term as well:

$$S(\{m_k, n_k\}) = -k_B N \sum_{k=0}^{q-1} (m_k \ln m_k + n_k \ln n_k). \quad (\text{B8})$$

To compute the free energy (per site), we must extremize  $E - TS$ :

$$\beta f(\beta, q) = \text{extr}_{\{m_k, n_k\}} \sum_{k=0}^{q-1} \left( m_k \ln m_k + n_k \ln n_k - \frac{\beta}{2} m_k n_k \right). \quad (\text{B9})$$

We apply the following ansatz, which assumes that symmetry will be broken in the  $k = 0$  spin direction:

$$m_0 = \frac{1}{q} [1 + (q-1)s], \quad (\text{B10})$$

$$m_k = \frac{1}{q} (1-s), \quad k = 1, 2, \dots, q-1, \quad (\text{B11})$$

$$n_0 = \frac{1}{q} [1 + (q-1)s], \quad (\text{B12})$$

$$n_k = \frac{1}{q} (1-s), \quad k = 1, 2, \dots, q-1. \quad (\text{B13})$$

There is now a single order parameter  $0 \leq s \leq 1$ , the spontaneous “magnetization” of the Potts model. We have:

$$\begin{aligned} \beta f(\beta, q) = \text{extr}_s & \left( \frac{2}{q} [1 + (q-1)s] \ln \left\{ \frac{1}{q} [1 + (q-1)s] \right\} \right. \\ & - \frac{\beta}{2} \left\{ \frac{1}{q} [1 + (q-1)s] \right\}^2 \\ & + \frac{2(q-1)}{q} (1-s) \ln \left[ \frac{1}{q} (1-s) \right] \\ & \left. - \frac{\beta(q-1)}{2} \left[ \frac{1}{q} (1-s) \right]^2 \right), \end{aligned} \quad (\text{B14})$$

which simplifies to

$$\begin{aligned} \beta f(\beta, q) = \text{extr}_s & \left\{ \frac{2}{q} [1 + (q-1)s] \ln [1 + (q-1)s] \right. \\ & + \frac{2(q-1)}{q} (1-s) \ln (1-s) \\ & \left. - 2 \ln q - \frac{\beta}{2q} [1 + (q-1)s^2] \right\}. \end{aligned} \quad (\text{B15})$$

This expression nearly coincides with the result for the complete graph in Ref. [44]. In particular,  $(2\gamma)f(2\gamma, q)$  on the complete bipartite graph is equal to  $\gamma f(\gamma, q)$  on the complete graph. An intuitive reason for this is that the “local neighborhood” of every vertex in the bipartite graph looks exactly like that of a complete graph, and the mean-field assumption ensures that this is all that matters.

Let  $s_*(\beta, q)$  be the value of  $s$  which extremizes the above, then  $s_*$  is the stable solution of

$$e^{\beta s_*(\beta, q)/2} = \frac{1 + (q-1)s_*(\beta, q)}{1 - s_*(\beta, q)}. \quad (\text{B16})$$

We now specialize to  $q = 1$ , which describes results for connectivity percolation. Now the order parameter  $s_*$ , which was the spontaneous “magnetization” in the Potts model, should be interpreted as the percolation probability, i.e.,

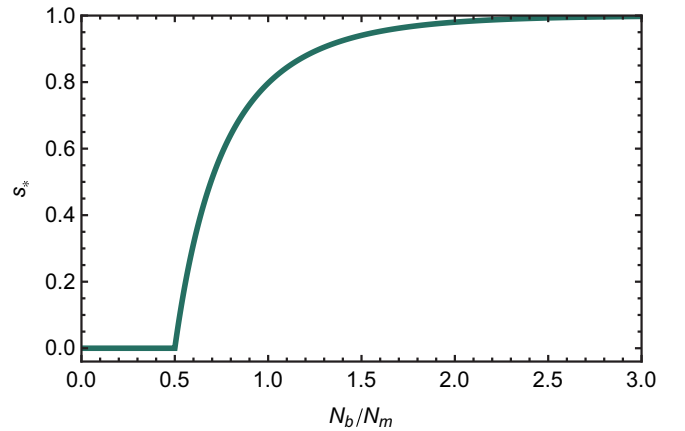


FIG. 15. (Color online) The bipartite graph percolation probability  $s_*$  as a function of  $N_b/N_M$ . A giant component appears continuously at  $N_b/N_M = 1/2$ —the singularity there is governed by the critical exponent  $\beta$ , which takes the mean-field percolation value 1.

the probability that a given site is connected to the giant component [45]. Translating further, into the language of rigidity on the regular square lattice,  $s_*$  is the probability that a given column or row shear mode is coupled to the “giant floppy mode.”

Our goal is now to compute the number of connected components on this bipartite graph, which we use in Eq. (B4) for the number of floppy modes. The result is

$$c(\gamma) = [1 - s_*(2\gamma, 1)] \left\{ 1 - \frac{\gamma}{2} [1 - s_*(2\gamma, 1)] \right\}. \quad (\text{B17})$$

Recall that we defined  $\gamma/L = p$ ; thus we have from Eq. (B16) that  $s_*(2pL, 1)$  satisfies  $1 - s_*(2pL, 1) = e^{-pLs_*(2pL, 1)}$ .

In our numerics we have been scaling the number of floppy modes by dividing by  $L$ . Here  $c$  was defined as the number of connected components *per vertex*, and so we divided by  $2L$  in its definition rather than  $L$ . Hence we must multiply  $c$  by 2 to

get  $\langle F \rangle / L$ . Thus the number of floppy modes is

$$\frac{\langle F \rangle}{L} = 2[1 - s_*(pL)] \left\{ 1 - \frac{pL}{2} [1 - s_*(pL)] \right\}, \quad (\text{B18})$$

with  $s_*(pL)$  satisfying  $1 - s_* = e^{-pLs_*}$ . The bipartite graph percolation probability  $s_*$  as a function of  $N_b/N_M$  [which with  $N_b$  translating to  $pL^2$  and  $N_M = 2(L + 1) - 3$  is equivalent to  $pL/2$  at large  $L$ ] is shown in Fig. 15. Note that there is a cusp at  $N_b/N_M = 1/2$ , and thus the appearance of the giant floppy mode is *not* at the Maxwell point. It may easily be shown from the mean-field equation for  $s_*$  that there is a finite slope at the transition, and this means that the critical exponent  $\beta$  governing the singularity there is equal to 1.

Figure 4(a) shows a comparison between the prediction for the floppy modes from Eq. (B18) (blue line) and the number of floppy modes measured for square grids with  $N = 100, 200$ , and 300.

- 
- [1] J. C. Phillips, *J. Non-Cryst. Solids* **34**, 153 (1979).  
 [2] M. Thorpe, *J. Non-Cryst. Solids* **57**, 355 (1983).  
 [3] S. Feng and P. N. Sen, *Phys. Rev. Lett.* **52**, 216 (1984).  
 [4] J. C. Phillips and M. F. Thorpe, *Solid State Commun.* **53**, 699 (1985).  
 [5] D. J. Jacobs and M. F. Thorpe, *Phys. Rev. Lett.* **75**, 4051 (1995).  
 [6] M. V. Chubynsky and M. F. Thorpe, *Phys. Rev. E* **76**, 041135 (2007).  
 [7] C. F. Moukarzel, *Phys. Rev. E* **68**, 056104 (2003).  
 [8] S. P. Kasiviswanathan, C. Moore, and L. Theran, in *Proceedings of the Twenty-second Annual ACM-SIAM Symposium on Discrete Algorithms (SODA 2011)*, edited by D. Randall (SIAM, Philadelphia, 2011), pp. 1237–1252.  
 [9] O. Rivoire and J. Barré, *Phys. Rev. Lett.* **97**, 148701 (2006).  
 [10] J. Barré, M. Lelarge, and D. Mitsche, [arXiv:1412.1004](https://arxiv.org/abs/1412.1004) [math.CO] (2014).  
 [11] P. M. Duxbury, D. J. Jacobs, M. F. Thorpe, and C. Moukarzel, *Phys. Rev. E* **59**, 2084 (1999).  
 [12] A. J. Liu and S. R. Nagel, *Nature* **396**, 21 (1998).  
 [13] A. J. Liu, S. R. Nagel, W. van Saarloos, and M. Wyart, in *Dynamical Heterogeneities in Glasses, Colloids, and Granular Media*, edited by L. Berthier, G. Biroli, J.-P. Bouchaud, L. Cipelletti, and W. van Saarloos (Oxford University Press, Oxford, 2010), Chap. 9.  
 [14] J. Schwarz, A. J. Liu, and L. Chayes, *Europhys. Lett.* **73**, 560 (2006).  
 [15] J. C. Maxwell, *Philos. Mag.* **27**, 294 (1864).  
 [16] X. Mao, N. Xu, and T. C. Lubensky, *Phys. Rev. Lett.* **104**, 085504 (2010).  
 [17] W. G. Ellenbroek and X. Mao, *Europhys. Lett.* **96**, 54002-p1 (2011).  
 [18] X. Mao and T. C. Lubensky, *Phys. Rev. E* **83**, 011111 (2011).  
 [19] T. C. Lubensky, C. L. Kane, X. Mao, A. Souslov, and K. Sun, [arXiv:1503.01324](https://arxiv.org/abs/1503.01324) [cond-mat.soft] (2015).  
 [20] C. Moukarzel and P. M. Duxbury, *Phys. Rev. E* **59**, 2614 (1999).  
 [21] C. Calladine, *Int. J. Solids Struct.* **14**, 161 (1978).  
 [22] C. L. Kane and T. C. Lubensky, *Nat. Phys.* **10**, 39 (2014).  
 [23] In a more rigorous classification, lattices satisfying  $z = 2d$  are called “Maxwell lattices” and only those ones with no self-stress are called “isostatic lattices.”  
 [24] K. Sun, A. Souslov, X. Mao, and T. C. Lubensky, *Proc. Natl. Acad. Sci. USA* **109**, 12369 (2012).  
 [25] E. D. Bolker and H. Crapo, *SIAM J. Appl. Math.* **36**, 473 (1979).  
 [26] L. E. Silbert, A. J. Liu, and S. R. Nagel, *Phys. Rev. Lett.* **95**, 098301 (2005).  
 [27] M. Wyart, L. E. Silbert, S. R. Nagel, and T. A. Witten, *Phys. Rev. E* **72**, 051306 (2005).  
 [28] S. D. Guest and J. W. Hutchinson, *J. Mech. Phys. Solids* **51**, 383 (2003).  
 [29] R. Connelly, P. Fowler, S. Guest, B. Schulze, and W. Whiteley, *Int. J. Solids Struct.* **46**, 762 (2009).  
 [30] J. Graver, B. Servatius, and H. Servatius, *Combinatorial Rigidity*, Graduate Studies in Mathematics, Vol. 2 (American Mathematical Society, Providence, RI, 1993).  
 [31] D. J. Jacobs and M. F. Thorpe, *Phys. Rev. E* **53**, 3682 (1996).  
 [32] D. J. Jacobs and B. Hendrickson, *J. Comput. Phys.* **137**, 346 (1997).  
 [33] G. Laman, *J. Eng. Math.* **4**, 331 (1970).  
 [34] L. Berthier and G. Biroli, *Rev. Mod. Phys.* **83**, 587 (2011).  
 [35] M. Mézard and G. Parisi, *J. Chem. Phys.* **111**, 1076 (1999).  
 [36] M. Aizenman and J. L. Lebowitz, *J. Phys. A* **21**, 3801 (1988).  
 [37] A. E. Holroyd, *Probab. Theory Relat. Fields* **125**, 195 (2003).  
 [38] J. P. Garrahan, P. Sollich, and C. Toninelli, in *Dynamical Heterogeneities in Glasses, Colloids, and Granular Media*, International Series of Monographs on Physics, Vol. 150, edited by L. Berthier, G. Biroli, J.-P. Bouchaud, L. Cipelletti, and W. van Saarloos (Oxford University Press, Oxford, 2011), Chap. 10, pp. 341–369.  
 [39] T. C. Lubensky and P. Chaikin, *Principles of Condensed Matter Physics* (Cambridge University Press, Cambridge, 2000).  
 [40] Strictly speaking, as we mentioned in the Introduction, bulk rigidity occurs at  $N_b = N_M - \mathcal{O}(1)$ , but for large lattices this point approaches  $N_b/N_M = 1$ .  
 [41] See Supplemental Material at <http://link.aps.org/supplemental/10.1103/PhysRevE.91.032124> for videos depicting the growth of rigid clusters and stressed regions in generic and regular lattices as braces are added to the simulated systems.  
 [42] W. Feller, *An Introduction to Probability Theory and Its Applications*, 3rd ed., Vol. I (John Wiley & Sons, Inc., New York, 1968) iX.3.d, pp. 224–225.  
 [43] I. Palásti, *Publ. Math. Inst. Hung. Acad. Sci.* **8**, 431 (1963).

- [44] A. Engel, R. Monasson, and A. K. Hartmann, *J. Stat. Phys.* **117**, 387 (2004).
- [45] F. Wu, *J. Stat. Phys.* **18**, 115 (1978).
- [46] D. Stauffer and A. Aharony, *Introduction to Percolation Theory*, 2nd ed. (Taylor & Francis, London, 1994).
- [47] A. Cayley, *Quart. J. Math.* **23**, 376 (1889).
- [48] L. Theran, in *Proceedings of the 21st Canadian Conference on Computational Geometry (CCCG2009)* (Vancouver, BC, 2009), pp. 63–66.
- [49] C. P. Goodrich, W. Ellenbroek, and A. J. Liu, *Soft Matter* **9**, 10993 (2013).
- [50] W. G. Ellenbroek, V. F. Hagh, A. Kumar, M. F. Thorpe, and M. van Hecke, [arXiv:1412.0273](https://arxiv.org/abs/1412.0273) [cond-mat.soft] (2014).
- [51] M. Wyart, *Ann. Phys. Fr* **30**, 1 (2005).
- [52] O. Stenull and T. C. Lubensky, *Phys. Rev. Lett.* **113**, 158301 (2014).
- [53] E. Teomy and Y. Shokef, *Phys. Rev. E* **86**, 051133 (2012).
- [54] F. Wu, *Rev. Mod. Phys.* **54**, 235 (1982).